Natural killer cell cytotoxicity shapes the clonal evolution of B cell leukaemia

Michelle C. Buri[1], Mohamed R. Shoeb[1], Aleksandr Bykov[1], Peter Repiscak[1], Hayeon Baik[1], Alma Dupanovic[1], Faith O. David[1,2], Boris Kovacic[1], Faith Hall-Glenn[1], Sara Dopa[1,3], Jos Urbanus[4], Lisa Sippl[1], Susanne Stofner[1], Dominik Emminger[1,5], Jason Cosgrove[6], Dagmar Schinnerl[1], Anna R. Poetsch[7], Manfred Lehner[1,5], Xaver Koenig[3], Leïla Perié[6], Ton N. Schumacher[4,8], Dagmar Gotthardt[9], Florian Halbritter[1], Eva M. Putz[1,2,#]

[1] St. Anna Children's Cancer Research Institute (CCRI), Vienna, Austria

[2] Center for Physiology and Pharmacology, Institute of Pharmacology, Medical University of Vienna, Vienna, Austria

[3] Center for Physiology and Pharmacology, Department of Neurophysiology and Pharmacology, Medical University of Vienna, Vienna, Austria

[4] Division of Molecular Oncology & Immunology, Oncode Institute, Netherlands Cancer Institute, Amsterdam, The Netherlands

[5] Christian Doppler Laboratory for Next Generation CAR T Cells, Vienna, Austria

[6] Institut Curie, Université PSL, Sorbonne Université, CNRS UMR168, Laboratoire Physico Chimie Curie, Paris, France

[7] Biomedical Genomics, Biotechnology Center, Center for Molecular and Cellular Bioengineering, Technische Universität Dresden, Germany

[8] Department of Hematology, Leiden University Medical Center, Leiden, The Netherlands.

[9] Institute of Pharmacology, University of Veterinary Medicine Vienna, Vienna, Austria

Correspondence to Eva M. Putz, Institute of Pharmacology, Medical University of Vienna, Waehringer Strasse 13A, 1090 Vienna, Austria, mail: eva-maria.putz@meduniwien.ac.at

Running title: NK cell killing shapes the clonal evolution of B-ALL in mice

Competing interest declaration: The authors declare no competing interests.

Word count: 241 (Abstract), 4933 (Introduction, Results, Discussion), 3739 (Materials and Methods)

Number of figures: 6

Number of supplementary figures: 8

Number of supplementary tables: 2

Keywords: cancer immunoediting, natural killer cells, tumour evolution, DNA barcoding, cytotoxicity, effector function, interferon-γ, perforin, Ly6A, LY6E

Abstract

The term cancer immunoediting describes the dual role by which the immune system can suppress and promote tumour growth and is divided into three phases: elimination, equilibrium and escape. The role of NK cells has mainly been attributed to the elimination phase. Here we show that NK cells play a role in all three phases of cancer immunoediting. Extended co-culturing of DNA barcoded mouse BCR/ABL^{p185+} B acute lymphoblastic leukaemia (B-ALL) cells with NK cells allowed for a quantitative measure of NK cell-mediated immunoediting. Whereas most tumour cell clones were efficiently eliminated by NK cells, a certain fraction of tumour cells harboured an intrinsic primary resistance. Furthermore, DNA barcoding revealed tumour cell clones with secondary resistance, which stochastically acquired resistance to NK cells. NK cell cytotoxicity put a selective pressure on B-ALL cells, which led to an outgrowth of primary and secondary resistant tumour cell clones, which were characterised by an IFN-γ signature. Besides well-known regulators of immune evasion, our analysis of NK cell resistant tumour cells revealed the upregulation of genes, including *Ly6a*, which we found to promote NK cell resistance in leukaemic cells. Translation of our findings to the human system showed that high expression of *LY6E* on tumour cells impaired the physical interaction with NK cells and led to worse prognosis in leukaemia patients. Our results demonstrate that tumour cells are actively edited by NK cells during the equilibrium phase and use different avenues to escape NK cell-mediated eradication.

48 # Introduction

49 Cancer immunoediting refers to the dynamic interaction between immune and cancer cells during
50 tumour development (1). The immune system can have both tumour-promoting and -suppressive
51 effects. This process occurs in three phases: elimination, equilibrium, and escape. In the elimination
52 phase, adaptive and innate immune cells, particularly cytotoxic T and natural killer (NK) cells, recognise
53 and eliminate cancer cells. The equilibrium phase involves the coexistence of tumour cells and the
54 immune system, leading to sculpting of the tumour under constant immune pressure, ultimately
55 resulting in immune escape (2).

56 NK cells are innate lymphoid cells with the ability of recognising and eliminating damaged, stressed,
57 and infected cells including cancer cells (3). NK cell activation relies on a balance of activating and
58 inhibitory signals from receptors on their surface during the interaction with potential target cells. On
59 the one hand, NK cells kill target cells through exocytosis of cytotoxic granules containing perforin and
60 granzymes (4), induction of death receptor-mediated apoptosis (5) or antibody-dependent cellular
61 cytotoxicity (6). On the other hand, NK cells secrete cytokines such as interferon-γ (IFN-γ), which
62 activate other immune cells in their vicinity (7). In the context of cancer immunoediting, NK cells play
63 a crucial role in eliminating tumour cells (8) and limiting their metastatic spread (9). NK cells spare
64 healthy tissue and represent a safe treatment option with minimal risk of causing adverse effects (10).
65 As a result, there is growing interest in using NK cells for immunotherapies, which will benefit from a
66 better understanding of how tumour cells evade NK cell attacks. Most studies to date have focused on
67 the interaction between human NK cells and tumour cell lines obtained from patients (11–16). These
68 tumour cells have already successfully evaded from the patient´s immune system and may thus not
69 represent suitable models to study immunoediting.

70 Here, we used an *in vitro* co-culture model based on non-edited NK cell-naïve mouse BCR/ABL^{p185+} B
71 cell acute lymphoblastic leukaemia (B-ALL) cells to investigate the primary interaction of tumour and
72 NK cells. NK cell resistant tumour cells that emerged during the co-culture showed an upregulation of
73 many IFN-γ-dependent genes, such as lymphocyte antigen 6 complex, locus A (*Ly6a*). This study

74 identified Ly6A as novel driver of NK cell-mediated immune evasion of mouse leukaemia and extended
75 our knowledge about the role of LY6E in limiting NK cell anti-tumour activity (17). Moreover, we
76 established a model to quantify NK cell effector functions and their ability to edit tumour cells by
77 cellular DNA barcoding (18–20). In summary, this study shows that NK cells play a role in all three
78 phases of cancer immunoediting and contribute to the active sculpting of tumour cells, ultimately
79 driving tumour evasion.

80 Material and methods

81 Mice

82 C57BL/6JRj wild-type mice (RRID:MGI:2670020) were obtained from the Janvier labs and C57BL/6-
83 Prf1^{tm1Sdz}/J (*Prf1*$^{-/-}$) (21) (Strain #002407, RRID:IMSR_JAX:002407) and B6.129S7-Ifng^{tm1Ts}/J (*Ifng*$^{-/-}$) (22)
84 mice (Strain #002287, RRID:IMSR_JAX:002287) were obtained from the Jackson Laboratory. B6.129-
85 B2m^{tm1Jae} (*B2m*$^{-/-}$, RRID:MGI:2175714) (23) mice were kindly provided by Thomas Kolbe (VetMedUni
86 Vienna). The mice were between 8 and 12 weeks of age and maintained under specific pathogen-free
87 conditions according to FELASA guidelines.

88 Cell culture

89 Phoenix-ECO (ATCC, RRID:CVCL_H717) and Lenti-X packaging cells (Takara, RRID:CVCL_1926) were
90 cultured in DMEM medium (Thermo Fisher Scientific) with 10% fetal bovine serum (FBS, Capricorn
91 Scientific). The K562 cell line (ATCC, RRID:CVCL_0004) was cultured in RPMI medium (Gibco)
92 supplemented with 100 U/ml penicillin and 100 µg/ml streptomycin (Gibco), 10% FBS and 50 µM β-
93 mercaptoethanol (Sigma-Aldrich) (cRPMI).
94 To generate BCR/ABL^{p185+} (B-ALL) cell lines, BM was isolated from 8-10-week-old mice and single cell
95 suspensions were prepared through repeated homogenisation using 18G and 24G needles. 48 hours
96 before the infection of BM cells, Phoenix-ECO cells were transiently transfected with a retroviral MSCV-
97 BCR/ABL^{p185} vector (kindly provided by Veronika Sexl) mixed with PureFection transfection reagent
98 (System Biosciences). The BM cells were transduced for 1 hour with the fresh viral supernatant in the

99 presence of 10 µg/ml polybrene (Sigma-Aldrich) and 10 ng/ml recombinant murine IL-7 (Peprotech).
100 Transformed B-ALL cells were maintained in cRPMI medium until they were stable cell lines
101 characterised by continuous growth and the homogenous expression of CD19, B220 and CD43 (approx.
102 2 months).
103 All cell lines were regularly tested for their mycoplasma negativity using the PCR Mycoplasma
104 detection kit (ABM). Cell growth and survival was measured using a CASY counter (OLS OMNI Life
105 Science) or a CellDrop BF (DeNovix).
106
107 Primary mouse NK (mNK) cells were isolated from spleens using the negative selection EasySep mouse
108 NK cell isolation kit (STEMCELL Technologies) or positive selection CD49b (DX5) MicroBeads kit
109 (Miltenyi Biotec) and cultured in cRPMI supplemented with 5,000 U/ml recombinant human IL-2 (rhIL-
110 2, Miltenyi Biotec). mNK cells were identified as single live mCD45.2^{+}mCD3^{-}NK1.1^{+}mCD335^{+} cells.
111 Human NK (hNK) cells were isolated from heathy donors with the negative selection kit, RosetteSep
112 Human NK Cell Enrichment Cocktail (Stemcell Technologies) and cultured in NK MACS medium
113 (Miltenyi Biotec) supplemented with 5% human serum (Capricorn Scientific) and 500 U/ml rhIL-2. hNK
114 cells were determined as single live hCD45^{+}hCD3^{-}CD56$^{\text{bright or dim}}$ cells.

115 ## DNA barcoding

116 **Generation of the lentiviral barcode library LG2.1**

117 The BC1DS_lib oligo containing a 21nt random barcode sequence (**Table S1**) was PCR amplified (14
118 cycles: 10 sec 98°C, 30 sec 57°C, 20 sec 72°C) with Phusion polymerase (New England Biolabs (NEB)).
119 The PCR amplified product was column purified (MinElute PCR cleanup kit, Qiagen) and subsequently
120 digested with XhoI and AscI, followed by ligation into the 3' UTR of the GFP cDNA sequence within the
121 pRRL lentiviral vector (24), using the Electroligase kit (NEB). Electrocompetent ElectroMax Stbl4
122 bacteria (Invitrogen) were electroporated with 6 ng ligation product and a small fraction of the
123 transformed bacteria was plated on Luria-Bertani (LB) agar plates to determine transformation
124 efficiency, while the remaining bacteria were grown overnight in 400 ml LB medium (VWR Life Science)

125 supplemented with 100 µg/ml ampicillin (Sigma-Aldrich). DNA was extracted from the bacterial culture
126 using the Maxiprep kit (Invitrogen). To determine the library's barcode diversity and distribution,
127 barcodes were amplified with a three PCR reaction protocol (see below) in biological and technical
128 duplicates and sequenced on a HiSeq 3000/4000 device (Illumina) with 64 bp single-end reads at the
129 Biomedical Sequencing Facility (BSF) Vienna.

130 **Barcoding of tumour cells**

131 Lenti-X cells were transfected with the LG2.1 barcode library and the two packaging plasmids p8.9QV
132 and pVSVG (25) (provided by Ton Schumacher) using the PureFection transfection reagent. Virus
133 supernatant was harvested after 48 and 72 hours and concentrated with AMICON columns (Sigma-
134 Aldrich). $2x10^5$ B-ALL cells were spinfected with serially diluted viral supernatant for 90 min at 900xg.
135 The transduction rate (%GFP^+ cells) was measured by flow cytometry 3 days after transduction.
136 Tumour cells with the desired transduction rate (<5% (18)) were expanded and FACS sorted to enrich
137 GFP^+ cells. Barcoded tumour cells were frozen for further experiments.

138 ## Flow cytometry

139 Cells were analysed on a FACSymphony A3 Cell Analyzer device (Becton Dickinson, BD) and sorted on
140 a FACSAria Fusion device (BD). The antibodies and cell stains used in this study are listed in **Table S2**.
141 Single living cells were gated according to size and granularity in FSC-A, SSC-A and FSC-H plots and cell
142 surface marker expression was quantified by median fluorescence intensity (MFI).

143 ***In vitro* co-culture system and tumour cell growth analysis**

144 $9x10^5$ barcoded B-ALL cells were co-cultured with mNK cells (4 days after isolation) in an effector-to-
145 target (E:T) ratio of 1:1 in three biological replicates per condition. Depending on NK cell cytotoxicity
146 and tumour cell growth, cells were harvested for FACS sorting and further analyses (described below)
147 on day 4-6 and 14-17. On the day of harvesting, $3x10^5$ tumour cells were co-cultured for a second or
148 third time with 4 day old mNK cells (E:T = 1:1). All conditions were cultured in the presence of 2,500
149 U/ml rhIL-2. In the experiment shown in **Figures 5A&S7A**, tumour cells were treated with 2 ng/ml
150 mouse IFN-γ (Abcam) every 2-3 days. During the co-culture, the absolute number of B-ALL tumour cells

151 was determined by flow cytometry using AccuCheck Counting Beads (Invitrogen). Tumour cells were
152 identified by gating on single live mCD45.2$^+$mCD19$^+$GFP$^+$ cells.

153 **Cytotoxicity assay**

154 5x10^4 CellTrace Violet (CTV, Invitrogen) stained B-ALL or K562 cells were seeded in 96-well round
155 bottom plates and IL-2-activated mNK or hNK cells added in the indicated E:T ratios in technical
156 duplicates or triplicates. After 1 or 4 hours of incubation at 37°C, cells were stained with fixable viability
157 dye eFluor 780 (Invitrogen) and fixed with fixation buffer (Biolegend) before flow cytometric analysis.
158 The percentage of specific NK cell lysis was calculated as follows: (% dead tumour cells after co-
159 incubation with NK cells - % spontaneous lysis) / (100 % - % spontaneous lysis).

160 **Effector function assay**

161 5x10^4 CTV$^+$ B-ALL or K562 cells were cultured with 5x10^4 IL-2 activated mNK or hNK cells, respectively.
162 As positive control served mNK or hNK cells stimulated with cell stimulation cocktail (Invitrogen) or 10
163 ng/ml IL-12 (Peprotech) + 100 ng/ml IL-15 (Peprotech) + 15 ng/ml IL-18 (R&D System), respectively. 1
164 hour after the start of co-culture, Brefeldin A (Biolegend) was added, and 3 hours later cells were fixed
165 with fixation buffer and permeabilized with intracellular staining permeabilization wash buffer
166 (Biolegend) before the intracellular staining of the cells for IFN-γ, granzyme B and TNF-α.

167 **Conjugation assay**

168 Tumour cells were stained with CTV and NK cells were either stained with anti-mNK1.1 or anti-hCD56.
169 An equal amount of tumour and NK cells was added into a FACS tube and cells were centrifuged for 3
170 min at 100xg. After no (human) or 10 min (mouse) incubation at 37°C, cells were vortexed for 3 sec
171 and fixed with ice cold 0.5% paraformaldehyde (Electron Microscopy Sciences) in PBS. Cells were kept
172 on ice and immediately measured by flow cytometry. Living cells were gated according to size and
173 granularity in FSC-A and SSC-A plots, doublets were included in the analysis, and CTV and CD56 or
174 NK1.1 double positive tumour-NK conjugates were quantified.

175 ## Multi-omics approaches

176 10^6 GFP^+ barcoded tumour cells were FACS sorted, washed twice with PBS and snap frozen. DNA and
177 RNA were extracted using the AllPrep DNA/RNA Mini Kit (Qiagen).

178 **DNA barcode sequencing**

179 Library preparation for barcode sequencing was performed in technical duplicates with three nested
180 PCR steps. PCR#1 amplified the barcodes, PCR#2 added the required sequences for the universal
181 Illumina adapters and four random base pairs (bps) for a more diverse sequencing start. PCR#3
182 attached the P5 and P7 universal Illumina adapters and with the P7 a sample-specific index sequence
183 (primer sequences are in **Table S1**). The samples were cleaned up with Agencourt AMPure XP beads
184 (Beckman Coulter). Up to 96 equimolar pooled samples spiked with 10-15% PhiX (Illumina) were
185 sequenced with the MiSeq Reagent Kit v3 (150 cycles) (Illumina) 64 bp single-end reads with a coverage
186 of 50-100 reads/barcode.

187 **Barcode/Cell clone evolution analysis**

188 The R statistics software v4.0.3 (RRID:SCR_001905) was used to analyse barcode abundance and clonal
189 diversity. Unmapped reads were loaded from FASTQ format (function *readDNAStringSet* from package
190 Biostrings v2.58.0, RRID:SCR_016949) into the R environment. Barcode sequences were located by
191 pattern matching (function *vmatchPattern* from package Biostrings v2.58.0) to identify the fixed head
192 ("GAACACTCGAGATCAG") and non-variable ("TGTGGTATGATGT") portions of the reads, which enclose
193 the barcodes from left and right, respectively. Sequences that did not meet the expected length (21
194 bases) or included uncalled bases ("N") were discarded (mean discarded sequences = 15%). To define
195 the barcodes of the reference library (**Figure S1C-E**), we selected sequences with a sum of at least 100
196 reads across samples (n = 4) of the viral library for further analysis. With these we constructed a count
197 matrix indicating the number of reads matching each barcode. Technical replicates were merged by
198 adding up the read counts. For each cell line, only barcodes detected across three B-ALL alone samples
199 at the corresponding reference timepoint with a total sum of at least 9 reads were considered for
200 downstream analysis. Barcode diversity for each sample was quantified using Shannon diversity as

201 follows $sum(p * log(p), na.rm = TRUE) * -1$, where p is the ratio of the counts of each barcode
202 relative to the total barcode counts. We used DESeq2 (RRID:SCR_015687) v1.30.0 to find the subset of
203 differentially abundant barcodes (absolute log_2(fold change_cutoff) ≥ 1 & padj < 0.05) between the
204 reference time point and conditions of interest. Shifted log_2 transformation was used for normalisation
205 (function *normTransform* from package DESeq2 v1.30.). Based on the statistics of differential
206 abundance and variability across samples (here, the variability was calculated as following: *v* =
207 $log2(max(x+1)/min(x+1))$, where x is a vector of normalised counts across samples) at every
208 time point, barcodes were assigned to one of five categories: i) primary resistant: differentially
209 abundant (padj < 0.05) and increasing (log_2(fold change) ≥ 1; comparing B-ALL + NK vs B-ALL alone); ii)
210 eliminated: differentially abundant (padj < 0.05) and decreasing (log_2(fold change) ≤ -1; comparing B-
211 ALL + NK vs B-ALL alone); iii) static: variability v ≤ 0.5 in B-ALL alone, and v < 1 at B-ALL + NK; iv)
212 secondary resistant: low variability v ≤ 0.5 in B-ALL alone, high variability in B-ALL + NK v ≥ 1 and
213 barcode abundance high in only one of the three replicates; v) others: none of the above. Barcodes
214 were further ordered using hierarchical clustering (function *hclust* from package *stats* v4.0.3*,* method
215 = "ward.d2", RRID:SCR_014673). Heatmaps were generated using ComplexHeatmap
216 (RRID:SCR_017270, v2.7.5.1) and bubble plots were generated using Matlab (RRID:SCR_001622).

217 **RNA sequencing**

218 After RNA isolation (see above), samples were treated with DNase I (Thermo Fisher Scientific). Library
219 preparation and sequencing was performed at the Biomedical Sequencing Facility (BSF) of the
220 Research Center for Molecular Medicine (CeMM) of the Austrian Academy of Sciences. RNA-seq
221 libraries were prepared with the QuantSeq 3' mRNA-Seq Library Prep Kit (FWD) for Illumina (Lexogen).
222 For sequencing, samples were pooled into NGS libraries in equimolar amounts. Expression profiling
223 libraries were sequenced on HiSeq 3000/4000 or Novaseq 6000 instruments (Illumina) following a 50-
224 , 100 and 120-base-pair single-end setup. Raw data acquisition and base calling was performed on-
225 instrument, while the subsequent raw data processing off the instruments involved two custom
226 programs based on Picard tools (RRID:SCR_006525, v2.19.2). In a first step, base calls were converted
227 into lane-specific, multiplexed, unaligned BAM files suitable for long-term archival

228 (IlluminaBasecallsToMultiplexSam, 2.19.2-CeMM). In a second step, archive BAM files were
229 demultiplexed into sample-specific, unaligned BAM files (IlluminaSamDemux, 2.19.2-CeMM).

230 **RNA-seq analysis**

231 Mapping of the reads was performed using STAR (26) (RRID:SCR_004463, v2.7.10a) to the *Mus*
232 *musculus* GRCm38, or *Homo sapiens* GRCh38 assemblies and duplicate reads were identified with
233 Picard (v2.27.4). Quantification of the mapped reads was carried out using Salmon (27)
234 (RRID:SCR_017036, v1.8.0). The following data processing and visualisation was performed in R
235 (v4.2.0). To ensure robustness of the analysis, the data set was filtered to include only transcripts
236 detected in at least three samples. The analyses of mouse cell lines A and B and cell lines C and D were
237 performed separately. Finally, the results were compared.

238 For count normalisation, variance stabilisation, and differential expression analysis, the Bioconductor
239 DESeq2 (28) (v1.38.3) package was used. DESeq2 employs a negative binomial distribution-based
240 model, with additional shrinkage using apeglm (29) or ashr algorithm (v1.20.0). Transcripts were
241 considered significantly differentially expressed between groups of comparison if they exhibited a
242 $\log_2$(fold change) ≥ 0.58 and a padj ≤ 0.05.

243 The principal component analysis (PCA), of expression heatmaps and volcano plots were generated
244 using ggplot2 (v3.4.2) and heatmap (v1.0.12). To correct for batch effects between different
245 experiments in PCA plots (**Figures S3A&B, S4A**) the limma R (30) package (RRID:SCR_010943, v3.54.2)
246 was utilised. The resulting gene lists were annotated and subjected to gene set enrichment analysis
247 (GSEA, RRID:SCR_003199). Visualisation of the GSEA results was achieved using the hypeR (31) package
248 (v2.0.1) and represented as dot plot. Gene Ontology Biological Process (GOBP) terms were obtained
249 from the Molecular Signatures Database (MSigDB) using the msigdbr (32) package (RRID:SCR_016863,
250 v7.5.1).

251 **ATAC sequencing**

252 $5x10^4$ GFP^+ tumour cells were FACS sorted into 1.5 ml micro centrifuge tubes containing 400 µl 0.5%
253 Bovine Serum Albumin (BSA, GE Healthcare) in PBS and pelleted. Cell lysis and DNA tagmentation was
254 performed in 25 µl tagment DNA enzyme in tagment DNA buffer (Illumina), 1% digitonin (Promega)

255 and EDTA-free protease inhibitor cocktail (Roche) for 30 min at 37°C. Samples were purified with the
256 Qiagen MinElute kit (Qiagen). Libraries were generated as described by Buenrostro et al (33) by using
257 the Ad1_noMx and Ad2.1-Ad2.48 indexed primers (**Table S1**). PCR products were purified with
258 Agencourt AMPure XP beads and the sample profile was analysed with the High Sensitivity D5000 kit
259 (Agilent Technologies) on a TapeStation (Agilent Technologies). 45-48 equimolar pooled samples were
260 sequenced on a NovaSeq 6000 instrument with 50 bp paired-end reads at the BSF (CeMM).

261 **ATAC-seq analysis**

262 The obtained raw reads were processed using the ATAC-seq Next Flow (34) pipeline (v2.0). This
263 included mapping the reads with STAR to the GRCm38 genome, identification of duplicates with Picard
264 (v2.27.4), calling broad peaks with MACS2 (35) (v2.2.7.1). Peaks overlapping with blacklisted (GRCh38)
265 regions were filtered out and the remaining peaks were annotated with HOMER (36)
266 (RRID:SCR_010881, v4.11). Consensus peaks across all samples were identified with BEDTools (37)
267 (RRID:SCR_006646, v2.30.0) and counting reads in these peaks was done with featureCounts (38)
268 (RRID:SCR_012919, Rsubread v2.0.1). Visualisation of the ATAC-seq peaks was performed by creation
269 of BigWig files with bedGraphToBigWig (v377) and exporting to the IGV (39) browser
270 (RRID:SCR_011793, v2.16.1). Quality of the obtained raw data was assessed with MultiQC (40)
271 (RRID:SCR_014982, v1.13). Data processing and visualisation was performed in R (v4.2.0). To ensure
272 robustness of the analysis, the data set was filtered to include only consensus peaks detected in all
273 three replicates of each condition and cell line and only the peaks that were located in the window of
274 ±3kb around the transcription start site (TSS). The analysis of cell lines A and B was performed
275 separately from the analysis of cell line C and D.

276 Similar to the RNA-seq analysis, the Bioconductor DESeq2 (1.38.3) package was used for count
277 normalisation, variance stabilisation, and analysis of differential accessibility. Peaks were considered
278 significantly accessible between groups of comparison if they exhibited a $\log_2$(fold change) ≥ 0.58 and
279 a padj ≤ 0.05. Exploratory analysis included PCA, production of heatmaps, volcano plots and GSEA.

280 **Integration of RNA-seq and ATAC-seq data**

281 To integrate two datasets and perform genome-wide quantification of differential transcription factor
282 activity in cell lines at different time points we used diffTF (41) (v1.8). The processing was done only
283 for A and B data sets, due to very high computational demand of the algorithm. The input consisted of
284 raw ATAC-seq reads in BAM files, filtered consensus peaks from the previous step, raw RNA-seq counts,
285 and PWM data for all TFs – HOCOMOCO (42) (RRID:SCR_005409, v10).

286 **2D-RP/RP Liquid Chromatography – Tandem Mass Spectrometry analysis**

287 Cells were lysed in 200 µL lysis buffer (50 mM HEPES pH 8.0, 2% SDS, 1 mM PMSF, cOmplete Protease
288 Inhibitor Cocktail, Roche), heated to 99 °C for 5 min, and DNA was sheared using a Covaris S2
289 ultrasonicator. Lysates were cleared at 20,000 × g for 15 min at 20 °C and tryptic digest was performed
290 using FASP according to Wisniewski et al (43). Peptides were desalted (C18 SPE; Pierce peptide
291 desalting columns, Thermo Fisher Scientific), labelled with TMTpro™ 16plex reagents (Thermo Fisher
292 Scientific), pooled, dried in a vacuum concentrator, and cleaned up via C18 SPE. After re-buffering in
293 10 mM ammonium formiate buffer pH 10, peptides were fractionated via a C18 column (150 × 2.0 mm
294 Gemini-NX, 3 µm, C18 110Å, Phenomenex, Torrance, CA, USA) on a Dionex UltiMate 3000 nanoLC
295 (Thermo Fisher Scientific). Fractions were dried in a vacuum concentrator and taken up in 0.1% TFA
296 before analysis.

297 Mass spectrometry analysis was performed on an Orbitrap Fusion Lumos Tribrid mass spectrometer
298 coupled to a Dionex UltiMate 3000 nanoLC system via a Nanospray Flex Ion Source (all from Thermo
299 Fisher Scientific) interface using the same procedure as Block et al (44). Data analysis was performed
300 using the Proteome Discoverer platform (RRID:SCR_014477, v.2.4.1.15).

301 Genome editing

302 **Ribonucleoprotein (RNP)-mediated CRISPR genome editing of B-ALL cells**

303 Cells were transfected with crRNAs, Alt-R CRISPR Cas9 tracrRNA ATTO 550 and Alt-R S.p. Cas9-GFP V3
304 (IDT) with the Gene Pulser Xcell electroporation system (BioRad) using the following settings: 350 V, 5
305 ms and 1 pulse. crRNA sequences: *Ly6a*: TCACGTTGACCTTAGTACCC; TATTGAAAGTATGGAGATCC,
306 *Plaat3*: CGTCATGTTTGTTATTGACC; ATGGCCCAGTGTCTGTACAT. The next day, GFP^{+}ATTO 550^{+} tumour

307 cells were FACS sorted. Cells were single cell FACS sorted into 96-well flat bottom plates into 50%
308 tumour cell conditioned medium and 50% fresh cRPMI. After the outgrowth of single clones, the KO
309 was validated by TIDE sequencing. Up to $2x10^5$ cells were lysed in 50 µl Pawel´s buffer at 56°C for 15
310 min with subsequent heat inactivation at 95°C for 5 min. After centrifugation at 2000xg for 5 min,
311 supernatant was used for the TIDE PCR to amplify the breakpoints of the guide RNAs (primer sequences
312 in **Table S1**). PCR products were Sanger sequenced (Microsynth) and analysed for their genotype with
313 the TIDE (nki.nl) web tool (RRID:SCR_023704). Gene knockouts were validated using flow cytometry or
314 quantitative PCR.

315 **CRISPR genome editing in Cas9 expressing K562 cell line**

316 K562 were transduced to express Cas9 with lentiviral supernatant from Lenti-X cells 48 hours after
317 transfection with the following constructs: lentiCRISPRv2 (RRID:Addgene_52961), p8.9QV and VSV-G
318 (both plasmids provided by T. Schumacher). K562 cells were transduced by spinfection for 90 min at
319 900xg. Transduced cells were selected with 1 µg/ml puromycin (Sigma-Aldrich) for up to 7 days. crRNA
320 specific for LY6E (GTGACTGTGTCTGCTAGTGC) was transfected into K562-Cas9 cells with the Gene
321 Pulser Xcell electroporation system using following settings: 400 V, 3 ms and 1 pulse. The cells were
322 single cell FACS sorted into 96-well flat bottom plates into 50% 48 hours old medium of tumour cells
323 and 50% fresh cRPMI with 100 Gray irradiated K562-mbIl15-41-BBL (kindly provided by Manfred
324 Lehner). After the outgrowth of single clones, the KO was validated by TIDE sequencing (primer
325 sequences in **Table S1**) and immunoblotting.

326 **Quantitative PCR**

327 To validate the *Plaat3*-deficiency in B-ALL cells, RNA was extracted from $2x10^6$ cells with the Monarch
328 Total RNA Miniprep Kit with "on column" DNase I treatment (NEB). cDNA was generated by using
329 LunaScript RT SuperMix Kit (NEB) and qPCR was performed with the Luna universal qPCR Master Mix
330 (NEB) (primer sequences in **Table S1**). The qPCR was conducted on a 7500 Real Time PCR System device
331 (Applied Biosciences) and the data was analysed with the 7500 Software v2.0.6.

332 **Immunoblotting**

333 To analyse LY6E protein expression, *LY6E* WT and KO cells were cultured with or without 10,000 U/ml
334 IFN-β (Miltenyi Biotec) or 10 ng/ml IFN-γ (Peprotech) overnight. Cells were lysed in RIPA buffer (Sigma-
335 Aldrich) with protease inhibitor cocktail (Thermo Scientific) and phosphatase inhibitor cocktail II
336 (Abcam). Equal amounts of protein were separated on a SDS polyacrylamide gel. Proteins were
337 transferred to a nitrocellulose membrane by using the Trans-Blot turbo transfer kit and system (Bio-
338 Rad). After blocking in 5% BSA-TBS-T, membranes were probed with primary antibodies against LY6E
339 (Invitrogen, RRID:AB_3075213) and β-actin (Cell Signaling Technologies, RRID:AB_2223172) overnight,
340 before the staining with a fluorescent secondary antibody (Thermo Scientific, RRID:AB_614946) and
341 visualisation by the ChemiDoc MP imaging system (Bio-Rad).

342 Seahorse – ATP rate assay

343 3.5 x10^4 *Ly6a* WT or KO cells were seeded in triplicates into the Seahorse XF HS PDL Miniplates (Agilent)
344 and centrifuged at 300xg for 2 min. The assay was conducted according to manufacturer's protocol,
345 measured on the Agilent Seahorse XF HS Mini Analyzer (Agilent) and analysed with the online Agilent
346 Seahorse Analytics software.

347 IFN-γ ELISA

348 Tumour cells were split to 3x10^5 cells/ml on day 0 and cultivated for 48 hours in cRPMI. On day 2, the
349 supernatant was harvested, filtered through a 45 µm filter, and transferred onto IL-2 expanded mNK
350 cells in the presence of 2,500 U/ml rhIL-2. After 48 hours, mNK cells were harvested and the
351 supernatant was frozen at -80°C. As positive control served the stimulation of mNK cells with cell
352 stimulation cocktail 4 hours before the supernatant harvesting. The ELISA was performed according to
353 manufactures protocol (Abcam) and analysed using the analysis tool:
354 "https://www.arigobio.com/elisa-analysis".

355 Statistical analysis

356 Statistical analysis was performed using GraphPad Prism (RRID:SCR_002798, v8.4.3 for Windows) using
357 two-tailed paired and unpaired t-tests, one-way, two-way ANOVA or Kruskal-Wallis tests as indicated.
358 Where ANOVA showed a statistical difference, Tukey's multiple comparison testing or Dunnett's post-

359 hoc testing was applied. The α level for all tests was set to 0.05, and p values were two tailed. The
360 significance level is indicated as following: *p < 0.05; **p < 0.01; ***p < 0.001; ****p < 0.0001.
361 To generate the heatmaps in Figure 1B&S1A, the data was pooled from 2-4 independent experiments
362 by calculating the mean surface marker expression or mean % specific lysis at E:T=10:1. The values
363 were standardised for each variable (row) using the following calculation: Z-score = (mean of observed
364 values – mean of the samples) / (standard deviation of the samples).
365 Heatmaps in Figures 5I&S7F were generated by using the R package ComplexHeatmap (v2.10.0). The
366 raw median fluorescence intensity (MFI) values minus the MFI of their unstained control served as
367 input. Rows (surface markers) were scaled and clustered (unsupervised). Columns (cell lines) were
368 ordered by genotype and cell line.

369 Data Availability

370 The data generated in this study are publicly available in Gene Expression Omnibus (GEO) at
371 GSE278011 (DNA barcode sequencing), GSE278010 (ATAC sequencing) and GSE278006 (RNA
372 sequencing). The computer codes for the data analysis are available on Github
373 (https://github.com/TumorImmunoEditingLab).

374 Results

375 Quantitative measure of NK cell effector functions

376 As a model to study NK cell evasion of leukaemic tumour cells we established a long-term *in vitro* co-
377 culture system using IL-2-activated primary mouse NK cells co-incubated with NK cell-naïve DNA
378 barcoded B-ALL cell lines for up to 20 days (**Figure 1A**). We generated several independent B-ALL cell
379 lines from the bone marrow (BM) of wild-type (WT, n=10) and major histocompatibility complex 1
380 (MHC-I)-deficient mice (*B2m*$^{-/-}$, n=10) and characterised their NK cell receptor ligand surface expression
381 and susceptibility towards NK cells. The two WT cell lines, which showed the highest susceptibility
382 towards NK cells (#13 and #15), expressed enhanced levels of the activating NKG2D-ligand Rae1 and
383 lower levels of inhibitory ligands (e.g. classical and non-classical MHC-I proteins H2-K^{b}, H2-D^{b}, Qa-1^{b}

384 and Qa-2) (**Figure 1B**). *B2m*$^{-/-}$ B-ALL cell lines showed a higher susceptibility towards NK cells according
385 to the recognition of missing self (45) (**Figure S1A**). To allow for a systematic quantification of NK cell
386 effector functions, a DNA barcode library was introduced into the WT B-ALL cell lines #13 and #15 (n=2
387 each) to track individual tumour cell clones over time. For this purpose, a new lentiviral barcode library
388 (LG2.1, containing 52,645 barcodes) was generated consisting of 21 random nucleotides positioned
389 downstream of a green fluorescent protein (*GFP*) gene (**Figures S1B-E**). The lentiviral library was
390 introduced into the B-ALL cell lines at a low multiplicity of infection to ensure the integration of a single
391 barcode per cell (25,46) (**Figure 1C**). To enrich for barcoded cells, GFP^{+} cells were FACS sorted shortly
392 after transduction and before the long-term co-culture with NK cells. The barcode diversity of the
393 resulting four cell lines called A and B (derived from #13), C and D (derived from #15) was determined
394 by site-specific PCR amplification and next generation sequencing (**Figure 1D**). The barcoded cells were
395 co-incubated with NK cells at an effector to target (E:T) ratio of 1:1. After 4 and 14 days, GFP^{+} tumour
396 cells were FACS purified and fresh NK cells were replenished to re-challenge the tumour cells.
397 Throughout the experiment, the absolute number of GFP^{+} tumour cells was determined by flow
398 cytometric analysis (**Figure 1E**). While the tumour cells initially showed significantly slower
399 proliferation in the presence of NK cells during the first two rounds of co-culture, this difference
400 became marginal in the third round. Twenty-nine days after the start of co-culture, we performed a
401 cytotoxicity assay. The extended co-culture of leukaemic cells with NK cells induced resistance towards
402 NK cell-mediated killing and led to tumour evasion *in vitro* (**Figure 1F**).

403 NK cell-mediated editing of leukaemic cells

404 There are four conceivable fates of B-ALL tumour cell clones upon long-term co-culture with NK cells:
405 The abundance of one clone could be lower ("eliminated"), higher ("primary resistant"), unchanged
406 ("static") or highly variable ("secondary resistant") (**Figure 2A**). After bulk DNA sequencing of the
407 barcodes, we designed a decision tree to discriminate these four categories algorithmically (**Figure 2B**).
408 Primary resistance, also known as intrinsic resistance (47), is defined as *a priori* resistance towards
409 therapy. In our study, primary resistance was characterised by a reproducible and significant

410 accumulation of a clone despite the presence of NK cells in co-culture. In comparison, secondary
411 resistance describes the phenomenon of acquired resistance, represented by a situation in which a
412 tumour can initially respond effectively to therapy but relapse or progress after treatment (48). We
413 hypothesised that secondary resistance was not a general tumour-intrinsic property but acquired only
414 by a subfraction of sibling cells and would therefore be observed only in isolated wells (**Figure 2A**).
415 Indeed, clustering of the barcoded leukaemic cells according to the pre-defined categories (**Figures**
416 **2C&D**), showed that the majority of clones was efficiently eliminated (58.5±4.8%, n=2-3 independent
417 experiments, n=2-4 B-ALL cell lines, mean±SD). A smaller number of cell clones showed an NK cell
418 resistant phenotype (14.3±4%) or remained static (23.9±4.4%) despite the presence of NK cells. As
419 hypothesised, we also observed secondary resistance, characterised by the presence of a cell clone in
420 only one of the three replicate wells (3.3±2.5%, **Figure 2E**). In line with the paradigm that the
421 acquisition of a resistant phenotype in tumour cells takes time, we observed the emergence of
422 secondary resistance primarily at the later of the two sampling timepoints (**Figure S2A**). To be able to
423 draw conclusions about the pre-existing fate of the tumour cell clones, we compared two independent
424 experiments with the same barcoded cell lines. As shown in **Figures 2F and S2B**, the cell clones
425 attributed to the clusters primary resistant and eliminated had the same fate in both experiments. In
426 contrast, the pool of secondary resistant tumour cell clones was distinctive for independent
427 experiments. In summary, whereas primary resistant and eliminated cells harboured tumour-intrinsic
428 properties *a priori* that determined their destiny, the fate of secondary resistant tumour cell clones
429 was stochastic. This underscored our hypothesis that secondary resistant tumour cells acquired their
430 resistant phenotype during NK cell co-culture. Our data clearly showed that apart from direct killing,
431 NK cells participated in immunoediting by actively shaping the tumourigenicity of individual tumour
432 cells.

433 Molecular changes observed in NK cell resistant B-ALL cells

434 To identify novel drivers of NK cell resistance we investigated changes in the transcriptomic and
435 chromatin accessibility profiles of NK cell resistant B-ALL cells generated during the long-term *in vitro*

436 co-culture. To this end, we performed RNA (**Figures 3A-D and S3**) and ATAC sequencing (**Figures 3E&F**
437 **and S4**) and compared NK cell co-cultured to NK cell naïve tumour cells. The transcriptomic analysis
438 showed a significant upregulation of genes with a well-known link to NK cell immune evasion such as
439 components of the MHC-I machinery (e.g., *Stat1*, *B2m*, *Tap1* and *H2-K1* (49)) (**Figures 3A and S3C**).
440 Additionally, this analysis revealed a novel set of genes, which may include potential drivers of NK cell
441 resistance, such as *Ly6a* and phospholipase A and acyltransferase 3 (*Plaat3*). The functional enrichment
442 analysis showed that the main biological process associated with the differentially expressed genes
443 (DEGs) was the response to IFN-γ (e.g., *Stat1*, *Irf1*, *Ccl5* and *Cd74*) (**Figure 3B**), which is produced by
444 activated NK cells in co-culture. After integrating the results from the four barcoded cell lines A-D, we
445 observed that many DEGs upon NK cell co-culture were cell line specific (up: A/B=193 and C/D=99,
446 down: A/B: 211 and C/D=63). However, a total of 129 genes were up- and 27 were downregulated in
447 all four cell lines and may be universally associated with or driving NK cell escape (**Figure 3C**). The top
448 30 DEGs are depicted in the heat map in **Figure 3D**. In line, the ATAC sequencing results showed the
449 opening of chromatin at the promoters of classical IFN-inducible genes (e.g., *Iigp1*, *Ifi27*, *Mx1*), as well
450 as of *Ly6a* and *Plaat3* (**Figures 3E and S4C**). We considered overlapping differentially accessible regions
451 (DARs) in cell lines A/B and C/D as the most robust ones (**Figure 3F**). Integration of RNA and ATAC
452 sequencing data by comparing the DEGs and DARs in cell lines A/B showed a significant intersection
453 (37 genes up/open, 16 genes down/closed). The two highly upregulated genes *Ly6a* and *Plaat3* in the
454 transcriptomic analysis were also present in this strictly filtered data set (**Figure 3G**). The quantification
455 of differential transcription factor (TF) activity by integrating the RNA and ATAC sequencing data sets
456 revealed TFs involved in NK cell resistance. We classified TFs as activators (NF2L1, SMRC1, JUN, IRF1
457 and IRF9) or repressors (RXRB, JUND), based on their expression and accessibility of predicted binding
458 sites (50). STAT1 expression was clearly upregulated but showed activating and repressive functions
459 and was therefore classified as undetermined (**Figure 3H**). A closer look at the top hits *Ly6a* and *Plaat3*
460 showed that both have multiple predicted binding sites for STAT1, IRF1 and IRF9 based on the
461 occurrence of DNA sequence motifs in the vicinity of accessible chromatin (**Figure 3I**). In summary,
462 multiomics analyses revealed that the B-ALL cells, which were not *a priori* sensitive and eliminated by

463 NK cells, showed a highly NK cell resistant phenotype characterised by a strong IFN-γ signature and the
464 upregulation of *Ly6a* and *Plaat3*.

465 Relative contribution of NK cell cytotoxicity and IFN-γ production in cancer 466 immunoediting

467 The two main functions of NK cells are the direct lysis of tumour cells and the production of pro-
468 apoptotic and -inflammatory cytokines, most importantly IFN-γ. To discriminate the relative
469 contributions of killing and cytokine production to cancer immunoediting, we performed two
470 independent long-term co-culture experiments with NK cells deficient in perforin (*Prf1*$^{-/-}$), which
471 renders them unable to kill their target cell (21), or deficient in IFN-γ production (*Ifng*$^{-/-}$) (**Figures 4, S5**
472 **and S6**). As described above, the growth of GFP^{+} tumour cells was measured by flow cytometry during
473 the experiment. On day 4 and 14 (for *Prf1*$^{-/-}$) or on day 4 and 17 (for *Ifng*$^{-/-}$), GFP^{+} tumour cells were
474 sorted and co-cultured with freshly prepared NK cells. As previously observed, B-ALL cells co-cultured
475 with WT NK cells showed an initial susceptibility during the first two weeks and developed an NK
476 resistance thereafter (**Figures 4A&C**). Co-culture with *Prf1*$^{-/-}$ NK cells only led to a minor growth
477 impairment of the tumour cells (**Figure 4A**). The presence of *Ifng*$^{-/-}$ NK cells diminished the number of
478 B-ALL cells in the beginning of the co-culture, but the tumour cells became resistant sooner than B-ALL
479 cells co-cultured with WT NK cells (**Figure 4C**). Five days after B-ALL cells outcompeted NK cells, we
480 measured their NK cell resistance. A cytotoxicity assay using WT NK cells was performed and showed
481 that in both experiments, B-ALL cells that had been co-cultured with WT NK cells showed the highest
482 NK cell resistance. *Prf1*$^{-/-}$ as well as *Ifng*$^{-/-}$ NK cell co-cultured B-ALL cells were more resistant compared
483 to B-ALL cells cultured alone, however the resistance was lower than in WT NK co-cultured B-ALL cells
484 (**Figures 4B&D**).
485 To study the clonal behaviour of the tumour cells, the B-ALL cells were analysed for their barcode
486 diversity on day 4 and 14/17. In line with our previous experiments, the barcode diversity of the B-ALL
487 + WT NK cell condition dropped significantly in both experiments by approx. 58%. The Shannon
488 diversity of B-ALL cells was decreased by 20% and 40% after co-culture with *Prf1*$^{-/-}$ or *Ifng*$^{-/-}$ NK cells,

489 respectively (**Figures 4E&G**). We observed a strong overlap of eliminated tumour cell clones in all
490 treatment groups, suggesting that these cell clones were *a priori* susceptible to NK cells. In line with
491 fewer eliminated cell clones, we detected more static B-ALL clones upon co-culture with *Prf1*$^{-/-}$ or *Ifng*$^{-}$
492 $^{/-}$ NK cells. The number of primary and secondary resistant tumour cell clones was similar after co-
493 culture with WT and *Ifng*$^{-/-}$ NK cells (**Figures 4H and S5A**). In contrast, the presence of *Prf1*$^{-/-}$ NK cells
494 led to a drastically lower number of primary and secondary resistant tumour cell clones (**Figures 4F**
495 **and S5B**). This suggested that the strong immunological pressure of NK cells leading to the emergence
496 of primary or secondary resistance was driven by cytotoxicity rather than IFN-γ production.
497 To define the molecular changes driving NK cell resistance, we compared the transcriptomic profiles
498 of B-ALL cells after co-culture with WT and *Prf1*$^{-/-}$ (day 14, **Figures 4I&J and S6A&B**) or *Ifng*$^{-/-}$ NK cells
499 (day 17, **Figures 4K&L and S6C&D** and day 32, **Figures S6E-H**). B-ALL cells after culture with WT or *Prf1*$^{-}$
500 $^{/-}$ NK cells showed an overlap of 28 up- and 18 downregulated DEGs, including *Ly6a* and *Plaat3* (**Figures**
501 **4I&J and S6A&B**). Intriguingly, B-ALL cells only showed marginal changes in their transcriptome when
502 cultured with *Ifng*$^{-/-}$ NK cells (**Figures 4K&L and S6C-H**). Accordingly, only B-ALL cells cultured in the
503 presence of IFN-γ-producing WT NK cells induced the expression of NK cell receptor ligands, such as
504 components of the classical and non-classical MHC-I machinery (**Figures S6I&J**).
505 In conclusion, while NK cell cytotoxicity was pivotal for the induction of primary and secondary
506 resistance in tumour cells, IFN-γ production induced an NK cell resistant phenotype on the
507 transcriptomic level. The combination of NK cell cytotoxicity and IFN-γ production was needed for
508 selecting and sculpting resistant tumour cells and ultimately for tumour immunoediting.

509 Role of PLAAT3 and Ly6A/LY6E in tumour evasion

510 NK cell resistance in B-ALL cells was associated with altered expression of well-known and novel genes
511 involved in cancer immunoediting. We demonstrated in multiple experiments that *Plaat3* and *Ly6a*
512 belonged to the most significantly upregulated genes in NK cell resistant B-ALL cell lines. Therefore, we
513 followed up on these genes and studied their role in immune evasion. We performed a co-culture
514 experiment as described in Figure 4A and analysed the B-ALL cells on day 14 by mass spectrometry to

515 confirm the upregulation of PLAAT3 and Ly6A on the protein level. Indeed, PLAAT3 and Ly6A were
516 increased after WT or *Prf1*$^{-/-}$ NK cell co-culture and even more upon recombinant IFN-γ treatment
517 (**Figures 5A and S7A**). We confirmed that the IFN-γ-dependent upregulation of Ly6A in B-ALL cells in
518 NK cell co-culture was stable, as it persisted several days after the NK cells were gone from the co-
519 culture (**Figure 5B**).
520 To study the role of PLAAT3 in more detail, we generated *Plaat3* KO B-ALL clones and verified the lack
521 of *Plaat3* mRNA by qPCR (**Figure S7B**). *Plaat3* KO cells did not show any difference in proliferation and
522 viability, IFN-γ production by NK cells and NK cell receptor ligand expression (**Figures S7C-F**). Moreover,
523 loss of *Plaat3* did not affect direct NK cell-mediated killing of mouse B-ALL cells (**Figure S7G**). To test
524 the relevance of the human orthologue *PLAAT3* in leukaemia, we analysed the *PLAAT3* expression of
525 ALL patients and observed an insignificant trend of worse overall survival in patients with increased
526 *PLAAT3* expression (**Figure S7H**). These results suggested that while PLAAT3 expression was
527 upregulated by IFN-γ and correlated with NK cell resistance, it does not constitute a driver of NK cell
528 resistance.
529 Likewise, we deleted *Ly6a* in B-ALL cells and verified the lack of Ly6A surface protein expression by
530 flow cytometry (**Figure 5C**). Ly6A deficiency had no impact on B-ALL cell proliferation or survival
531 (**Figures 5D&E**). To investigate the impact of Ly6A on the transcriptomic level, we performed RNA
532 sequencing of *Ly6a* WT and KO B-ALL cells and found 127 up- and 80 downregulated genes mainly
533 related to metabolic processes (**Figures 5F&G**). In line with these results, we observed an increased
534 mitochondrial and glycolytic ATP production in *Ly6a* KO cells (**Figure 5H**). Increased tumour
535 metabolism may induce stress ligand expression and consequently lead to better activation of NK cells
536 (51). While the majority of classical NK cell receptor ligands showed unaltered expression, we observed
537 a slightly higher expression of Rae1 ($p=0.08$, unpaired *t*-test) and lower expression of CD112 ($p=0.04$)
538 in B-ALL cells lacking Ly6A (**Figure 5I).** Further, CD244 was upregulated in *Ly6a* KO cells on RNA and
539 protein level (**Figures 5F&J**), a marker known to be present on NK cells (52), but only basally expressed
540 in mouse marginal-zone B cells (53) with a reported function in B cell differentiation and autoimmunity
541 (54). We tested the functional consequences of *Ly6a* deficiency for the interaction of B-ALL and NK

542 cells. We detected unaltered IFN-γ (**Figure 5K**) and granzyme B production (**Figure 5L**) upon co-culture
543 with B-ALL cells and similar numbers of tumour-NK conjugates (**Figure 5M**) irrespective of the presence
544 or absence of *Ly6a*. However, *Ly6a* KO B-ALL cells were more susceptible to NK cells compared to WT
545 cells in cytotoxicity assays (**Figure 5N**). These results clearly show that Ly6A plays an important role in
546 NK cell-mediated immune evasion of mouse B-ALL cells.
547 LY6E has been well-described as close relative of Ly6A in the human system (55). High *LY6E* expression
548 correlated significantly with poor survival in ALL patients (**Figure 6A**). To further study the human
549 relevance of our findings, we generated *LY6E*-deficient BCR/ABL1^{+} K562 cells and verified the lack of
550 LY6E protein expression by immunoblotting. Notwithstanding that others have seen an IFN-β and IFN-
551 γ-dependent induction of LY6E expression in hematopoietic cells (55), we only detected an
552 upregulation of LY6E using IFN-β (**Figure 6B**). Transcriptomic analysis of *LY6E* WT and KO K562 cells
553 showed a total of 829 deregulated genes (454 up and 375 down, **Figure 6C**), which were mainly
554 associated to cell death, cell cycle and intracellular transport (**Figure 6D**). However, we did not observe
555 any significant differences in cell proliferation nor viability between *LY6E* WT and KO clones (**Figures**
556 **6E&F**). When analysing the interaction of NK cells with *LY6E* WT and KO clones we found no difference
557 in NK cell IFN-γ and TNF-α production (**Figure S8**), but a tendency for an increased NK cell susceptibility
558 of the *LY6E* KO clones (**Figure 6G**). More strikingly, we detected that *LY6E* KO clones formed
559 significantly more tumour-NK conjugates compared to *LY6E* WT cells (**Figure 6H**).
560 In summary, our functional analysis of PLAAT3 and Ly6A showed that their expression is upregulated
561 in tumour cells co-cultured with NK cells in an IFN-γ-dependent manner. Although PLAAT3 was
562 persistently upregulated in our multiomics analysis, it proved to have no effect on NK cell resistance.
563 In contrast, Ly6A/LY6E were identified as a novel drivers of tumour evasion by impairing the interaction
564 of NK and tumour cells.
565

566 # Discussion

567 NK cells represent a potent arm of the immune system, tasked with eliminating malignant cells.
568 Nonetheless, they can fail controlling cancer cells which successfully evaded from the immune
569 surveillance. The presented study aimed to elucidate the mechanisms employed by tumour cells to
570 escape NK cells. Our study is based on heterogeneous, non-edited and immune-naïve mouse
571 BCR/ABL^{p185+} B-ALL tumour cell lines, which were co-cultured for several weeks with mouse NK cells.
572 This unique model enables to explore the primary interplay between tumour cells and the immune
573 system. Furthermore, the B-ALL tumour cells were DNA barcoded, a technique that allows for the
574 quantification of tumour cell clonal dynamics and a better understanding of NK cell effector functions.
575 To the best of our knowledge, this particular aspect has not been demonstrated in previous studies.
576 The determination of tumour cell fate during the co-culture revealed that most tumour cell clones
577 possessed inherent sensitivity or resistance to NK cells. This technique has already been used by many
578 others to quantify tumour cell susceptibility towards immune cells, drug- or antibody-based
579 immunotherapies (56–59). Similar to our research, these studies observed that the majority of tumour
580 cells is predestined for being sensitive or resistant to treatment. Our study highlighted tumour cell
581 clones beyond those two fundamental fates of life and death, which acquired secondary resistance in
582 the presence of NK cells. Secondary resistance, defined as the occurrence of resistance in one of three
583 replicate wells after two weeks of co-culture, was only observed in a small subset of tumour cell clones.
584 Similarly, using DNA barcoding to investigate the clonal evolution of drug-treated lung cancer cells,
585 Acar *et al.* recently described the emergence of "*de novo* resistant lineages" in one replicate only (56).
586 Interestingly, we found that secondary resistant tumour cells were highly distinctive for each
587 independently performed experiment, suggesting that a stochastic event causes the resistance.
588 However, due to the necessity of expanding the barcoded cell lines before the experiments (to ensure
589 reproducible representation of all barcodes in every well), we cannot formally exclude the possibility
590 of pre-existing heterogeneity within a cell clone. Furthermore, the barcode sequence of the LG2.1
591 library was found to be located approximately 900 bps upstream of the polyA tail and could thus not

592 be detected using single-cell RNA sequencing. It would certainly be interesting to delve deeper into
593 secondary resistance mechanisms and to compare the transcriptomic profiles of primary and
594 secondary resistant tumour cell clones in the future (60,61).
595 In summary, the DNA barcode analysis demonstrated that NK cells can shape tumour cells and
596 contribute to immunoediting of tumour cell clones. To dissect the two main functions of NK cells,
597 namely killing tumour cells and producing IFN-γ, we analysed the clonal evolution of B-ALL cells co-
598 cultured with *Prf1*$^{-/-}$ and *Ifng*$^{-/-}$ NK cells, respectively. It is widely acknowledged that IFN-γ is a major
599 player in cancer immunoediting (62). In our experiments, tumour cells responded to the NK cell co-
600 culture with an upregulation of many IFN-γ inducible genes, such as MHC-I molecules, thereby
601 inhibiting NK cells and inducing resistance. Interestingly, and against our expectations, we observed a
602 similar number of primary and secondary resistant B-ALL cell clones upon co-culture with WT or *Ifng*$^{-/-}$
603 NK cells. On the contrary, co-culture with *Prf1*$^{-/-}$ NK cells led to fewer primary and secondary resistant
604 B-ALL cell clones. This clearly suggested that the selection of *a priori* resistant tumour cell clones and
605 the acquisition of secondary resistance was mainly mediated by NK cell killing rather than IFN-γ
606 production. However, the transcriptomic changes observed in long-term co-cultured B-ALL cells were
607 only partially affected by loss of NK killing capacity, but completely absent in B-ALL cells cultured with
608 *Ifng*$^{-/-}$ NK cells. This data argues against a major contribution of other NK cell-derived cytokines such as
609 TNF-α on the tumour immunoediting process. We thus concluded that while IFN-γ plays only a minor
610 role in tumour cell elimination, it enhances NK cell resistance of the remaining tumour cells by
611 upregulating IFN-γ dependent genes, such as genes involved in MHC-I presentation and *Ly6a*.
612 Amongst others, previously described NK cell tumour evasion mechanisms include the upregulation of
613 proteins involved in antigen presentation and MHC-I and -II molecules (63,64), the loss or shedding of
614 NKG2D ligands such as MHC class I chain-related molecule A and B (MICA/B) (65) and secretion of TGF-
615 β and IL-10 (66). Notably, we here describe *Ly6a* overexpression as emerging novel driver of tumour
616 evasion by impairing NK cell-mediated killing. Ly6A, also called stem cell antigen-1 (Sca-1), is an 18-kDa
617 mouse glycosylphosphatidylinositol-anchored cell surface protein. It plays an important role in
618 haematopoietic progenitor/stem cell lineage fate, brain blood barrier transport and cancer stem cell

619 biology (67–70). Ly6A was shown to be upregulated in cancer stem cells and many tumour entities and
620 is induced by Wnt/β-Catenin signalling and TGF-β deregulation. This promotes cell adhesion and
621 migration *in vitro,* increased tumourigenicity and resistance to chemotherapy *in vivo* (70–73). The
622 human LY6 gene family comprises several members, but the direct orthologue of mouse *Ly6a* has been
623 under debate for a long time. *LY6A/LY6S* was just recently discovered probably due to its genomic
624 localisation on the opposite strand of and highly overlapping with *C8orf3/LINC02904* (55,74). The
625 expression of *LY6A/LY6S* seems to be restricted to pituitary tumours (74) and a subset of non-classical
626 lymphoid cells of the spleen (55), and it could not be detected in hematopoietic cell lines (74) or cancer
627 patients. Besides *LY6A/LY6S*, other *LY6* family members were suggested as close homologues of the
628 murine *Ly6a* gene, such as *LY6D*, *LY6E*, *LY6H* and *LY6K*, which were implicated as novel biomarkers for
629 poor cancer prognosis and are frequently amplified in human cancer (75). Al Hossiny *et al.* showed that
630 human LY6E promotes breast cancer *in vivo* and drives drug sensitivity and epithelial-to-mesenchymal
631 transition. Moreover, they observed that LY6E is required for TGF-β signalling and facilitates immune
632 evasion by upregulating PD-L1 on cancer cells, by recruiting T-regulatory cells and dampening NK cell
633 activation (17). In line, our survival analysis of a paediatric ALL-patient cohort confirmed the cancer
634 driving feature of LY6E also in leukaemia. Our data clearly shows that NK cells are less likely to form
635 conjugates with human leukemic cells in the presence of LY6E, which ultimately resulted in a minor
636 increase in NK cell susceptibility. In summary, this substantiates the reported oncogenic and immune
637 suppressive properties of human LY6E and murine Ly6A, but the exact mechanism remains unknown.
638 Although Ly6A has not been directly associated with cell metabolism, our data indicates that *Ly6a* KO
639 B-ALL cells produce more ATP through glycolysis and oxidative phosphorylation. Increased metabolism
640 is generally associated with immune suppression and NK cell inhibition (76), which is contradictory to
641 our observed phenotype. However, it was also shown that increased glycolysis can enhance the
642 expression of NK cell activating NKG2D ligands (51). We only observed a slight and insignificant
643 increase of Rae1 on *Ly6a* KO B-ALL cells, besides differences in CD112 and CD244 expression. It has
644 been suggested that Ly6A regulates the clustering of receptors or ligands within lipid rafts on the cell
645 membrane (77). We thus hypothesise that potential differences in local concentrations of NK cell

receptor ligands may contribute to the lower susceptibility of Ly6A-expressing B-ALL cells to NK cell-mediated killing, but this notion needs further evaluation.

Considering the association of *Ly6a* with cancer stemness, our findings align with the concept that immunoedited and thus more aggressive tumour cells may harbour cancer stem cell (CSC) features. CSCs are considered responsible for metastasis and therapy resistance, as they are characterised by deregulated differentiation, self-renewal, drug resistance, and amongst others evasion of immunosurveillance. Unlike other immune cells, NK cells are believed to show direct cytotoxicity against CSCs (78). On the other hand, as CSCs frequently upregulate classical and non-classical MHC-I molecules while losing NK cell activating ligands, it is still a matter of debate if and how NK cells are able to detect and kill CSCs (78,79).

In conclusion, our work sheds light on the intricate interplay between NK and leukaemic cells during initial encounters. This study shows that leukaemic cells are actively shaped by NK cells and unravels novel cancer evasion strategies by identifying potential driver genes in mice (*Ly6a*) and men (*LY6E*). Further research, especially *in vivo* and with single cell resolution, is required to delve deeper into primary and secondary resistance mechanisms and the general role of Ly6A and LY6E in NK cell-mediated tumour surveillance. These findings ultimately deepen our understanding of the initial interaction between tumour and NK cells and of cancer immune evasion in general.

663 # References:

664 1. Gubin MM, Vesely MD. Cancer Immunoediting in the Era of Immuno-oncology. Clin Cancer Res.
665 2022;28:3917–28.

666 2. Dunn GP, Bruce AT, Ikeda H, Old LJ, Schreiber RD. Cancer immunoediting: from
667 immunosurveillance to tumor escape. Nat Immunol. Nature Publishing Group; 2002;3:991–8.

668 3. Wolf NK, Kissiov DU, Raulet DH. Roles of natural killer cells in immunity to cancer, and
669 applications to immunotherapy. Nat Rev Immunol. Nature Publishing Group; 2023;23:90–105.

670 4. Metkar SS, Wang B, Aguilar-Santelises M, Raja SM, Uhlin-Hansen L, Podack E, et al. Cytotoxic Cell
671 Granule-Mediated Apoptosis: Perforin Delivers Granzyme B-Serglycin Complexes into Target
672 Cells without Plasma Membrane Pore Formation. Immunity. Elsevier; 2002;16:417–28.

673 5. Prager I, Watzl C. Mechanisms of natural killer cell-mediated cellular cytotoxicity. J Leukoc Biol.
674 2019;105:1319–29.

675 6. Wang W. NK cell-mediated antibody-dependent cellular cytotoxicity in cancer immunotherapy.
676 Front Immunol [Internet]. 2015 [cited 2023 Jul 20];6. Available from:
677 http://journal.frontiersin.org/Article/10.3389/fimmu.2015.00368/abstract

678 7. Bald T, Krummel MF, Smyth MJ, Barry KC. The NK cell–cancer cycle: advances and new challenges
679 in NK cell–based immunotherapies. Nat Immunol. 2020;21:835–47.

680 8. O'Sullivan T, Saddawi-Konefka R, Vermi W, Koebel CM, Arthur C, White JM, et al. Cancer
681 immunoediting by the innate immune system in the absence of adaptive immunity. J Exp Med.
682 2012;209:1869–82.

683 9. López-Soto A, Gonzalez S, Smyth MJ, Galluzzi L. Control of Metastasis by NK Cells. Cancer Cell.
684 Elsevier; 2017;32:135–54.

685 10. Liu E, Marin D, Banerjee P, Macapinlac HA, Thompson P, Basar R, et al. Use of CAR-Transduced
686 Natural Killer Cells in CD19-Positive Lymphoid Tumors. N Engl J Med. Massachusetts Medical
687 Society; 2020;382:545–53.

688 11. Bernareggi D, Xie Q, Prager BC, Yun J, Cruz LS, Pham TV, et al. CHMP2A regulates tumor sensitivity
689 to natural killer cell-mediated cytotoxicity. Nat Commun. 2022;13:1899.

690 12. Chiba M, Shimono J, Ishio T, Takei N, Kasahara K, Ogasawara R, et al. Genome-wide CRISPR
691 screens identify CD48 defining susceptibility to NK cytotoxicity in peripheral T-cell lymphomas.
692 Blood. 2022;140:1951–63.

693 13. Pech MF, Fong LE, Villalta JE, Chan LJ, Kharbanda S, O'Brien JJ, et al. Systematic identification of
694 cancer cell vulnerabilities to natural killer cell-mediated immune surveillance. eLife.
695 2019;8:e47362.

696 14. Sheffer M, Lowry E, Beelen N, Borah M, Amara SNA, Mader CC, et al. Genome-scale screens
697 identify factors regulating tumor cell responses to natural killer cells. Nat Genet. Nat Genet;
698 2021;53:1196–206.

699 15. Carré T, Thiery J, Janji B, Terry S, Gros G, Meurice G, et al. Selection of tumor-resistant variants
700 following sustained natural killer cell-mediated immune stress. Oncol Rep. 2021;45:582–94.

701 16. Dufva O, Gandolfi S, Huuhtanen J, Dashevsky O, Duàn H, Saeed K, et al. Single-cell functional
702 genomics reveals determinants of sensitivity and resistance to natural killer cells in blood
703 cancers. Immunity. 2023;56:2816-2835.e13.

704 17. Al Hossiny M, Luo L, Frazier WR, Steiner N, Gusev Y, Kallakury B, et al. Ly6E/K signaling to TGF-β
705 promotes breast cancer progression, immune escape and drug resistance. Cancer Res.
706 2016;76:3376–86.

707 18. Naik SH, Schumacher TN, Perié L. Cellular barcoding: A technical appraisal. Exp Hematol.
708 2014;42:598–608.

709 19. Eisele AS, Cosgrove J, Magniez A, Tubeuf E, Tenreira Bento S, Conrad C, et al. Erythropoietin
710 directly remodels the clonal composition of murine hematopoietic multipotent progenitor cells.
711 eLife. 2020;11:e66922.

712 20. Marsolier J, Prompsy P, Durand A, Lyne A-M, Landragin C, Trouchet A, et al. H3K27me3 conditions
713 chemotolerance in triple-negative breast cancer. Nat Genet. 2022;54:459–68.

714 21. Kägi D, Ledermann B, Bürki K, Seiler P, Odermatt B, Olsen KJ, et al. Cytotoxicity mediated by T
715 cells and natural killer cells is greatly impaired in perforin-deficient mice. Nature. 1994;369:31–
716 7.

717 22. Dalton DK, Pitts-Meek S, Keshav S, Figari IS, Bradley A, Stewart TA. Multiple defects of immune
718 cell function in mice with disrupted interferon-gamma genes. Science. 1993;259:1739–42.

719 23. Zijlstra M, Bix M, Simister NE, Loring JM, Raulet DH, Jaenisch R. Beta 2-microglobulin deficient
720 mice lack CD4-8+ cytolytic T cells. Nature. 1990;344:742–6.

721 24. Dull T, Zufferey R, Kelly M, Mandel RJ, Nguyen M, Trono D, et al. A Third-Generation Lentivirus
722 Vector with a Conditional Packaging System. J Virol. American Society for Microbiology;
723 1998;72:8463–71.

724 25. Eisele AS, Cosgrove J, Magniez A, Tubeuf E, Tenreira Bento S, Conrad C, et al. Erythropoietin
725 directly remodels the clonal composition of murine hematopoietic multipotent progenitor cells.
726 eLife. 2022;11:e66922.

727 26. Dobin A, Davis CA, Schlesinger F, Drenkow J, Zaleski C, Jha S, et al. STAR: ultrafast universal RNA-
728 seq aligner. Bioinformatics. 2013;29:15–21.

729 27. Patro R, Duggal G, Love MI, Irizarry RA, Kingsford C. Salmon: fast and bias-aware quantification
730 of transcript expression using dual-phase inference. Nat Methods. 2017;14:417–9.

731 28. Love MI, Huber W, Anders S. Moderated estimation of fold change and dispersion for RNA-seq
732 data with DESeq2. Genome Biol. 2014;15:550.

733 29. Zhu A, Ibrahim JG, Love MI. Heavy-tailed prior distributions for sequence count data: removing
734 the noise and preserving large differences. Stegle O, editor. Bioinformatics. 2019;35:2084–92.

735 30. Ritchie ME, Phipson B, Wu D, Hu Y, Law CW, Shi W, et al. limma powers differential expression
736 analyses for RNA-sequencing and microarray studies. Nucleic Acids Res. 2015;43:e47.

737 31. Federico A, Monti S. hypeR: an R package for geneset enrichment workflows. Bioinformatics.
738 2019;36:1307–8.

739 32. Liberzon A, Birger C, Thorvaldsdóttir H, Ghandi M, Mesirov JP, Tamayo P. The Molecular
740 Signatures Database (MSigDB) hallmark gene set collection. Cell Syst. 2015;1:417–25.

741 33. Buenrostro JD, Wu B, Chang HY, Greenleaf WJ. ATAC-seq: A Method for Assaying Chromatin
742 Accessibility Genome-Wide. Curr Protoc Mol Biol [Internet]. 2015 [cited 2023 Mar 22];109.
743 Available from: https://onlinelibrary.wiley.com/doi/10.1002/0471142727.mb2129s109

744 34. Ewels PA, Peltzer A, Fillinger S, Patel H, Alneberg J, Wilm A, et al. The nf-core framework for
745 community-curated bioinformatics pipelines. Nat Biotechnol. Nature Publishing Group;
746 2020;38:276–8.

747 35. Gaspar JM. Improved peak-calling with MACS2 [Internet]. bioRxiv; 2018 [cited 2023 Oct 25]. page
748 496521. Available from: https://www.biorxiv.org/content/10.1101/496521v1

749 36. Heinz S, Benner C, Spann N, Bertolino E, Lin YC, Laslo P, et al. Simple combinations of lineage-
750 determining transcription factors prime cis-regulatory elements required for macrophage and B
751 cell identities. Mol Cell. 2010;38:576–89.

752 37. Quinlan AR, Hall IM. BEDTools: a flexible suite of utilities for comparing genomic features.
753 Bioinforma Oxf Engl. 2010;26:841–2.

754 38. Liao Y, Smyth GK, Shi W. featureCounts: an efficient general purpose program for assigning
755 sequence reads to genomic features. Bioinformatics. 2014;30:923–30.

756 39. Thorvaldsdóttir H, Robinson JT, Mesirov JP. Integrative Genomics Viewer (IGV): high-
757 performance genomics data visualization and exploration. Brief Bioinform. 2013;14:178–92.

758 40. Ewels P, Magnusson M, Lundin S, Käller M. MultiQC: summarize analysis results for multiple tools
759 and samples in a single report. Bioinformatics. 2016;32:3047–8.

760 41. Berest I, Arnold C, Reyes-Palomares A, Palla G, Rasmussen KD, Giles H, et al. Quantification of
761 Differential Transcription Factor Activity and Multiomics-Based Classification into Activators and
762 Repressors: diffTF. Cell Rep. Elsevier; 2019;29:3147-3159.e12.

763 42. Kulakovskiy IV, Vorontsov IE, Yevshin IS, Soboleva AV, Kasianov AS, Ashoor H, et al. HOCOMOCO:
764 expansion and enhancement of the collection of transcription factor binding sites models.
765 Nucleic Acids Res. 2016;44:D116–25.

766 43. Wiśniewski JR, Zougman A, Nagaraj N, Mann M. Universal sample preparation method for
767 proteome analysis. Nat Methods. 2009;6:359–62.

768 44. Block J, Rashkova C, Castanon I, Zoghi S, Platon J, Ardy RC, et al. Systemic Inflammation and
769 Normocytic Anemia in DOCK11 Deficiency. N Engl J Med. 2023;

770 45. Kärre K, Ljunggren HG, Piontek G, Kiessling R. Selective rejection of H–2-deficient lymphoma
771 variants suggests alternative immune defence strategy. Nature. Nature Publishing Group;
772 1986;319:675–8.

773 46. Naik SH, Perié L, Swart E, Gerlach C, van Rooij N, de Boer RJ, et al. Diverse and heritable lineage
774 imprinting of early haematopoietic progenitors. Nature. 2013;496:229–32.

775 47. Bai R, Chen N, Li L, Du N, Bai L, Lv Z, et al. Mechanisms of Cancer Resistance to Immunotherapy.
776 Front Oncol. 2020;10:1290.

48. Sharma P, Hu-Lieskovan S, Wargo JA, Ribas A. Primary, Adaptive, and Acquired Resistance to Cancer Immunotherapy. Cell. Elsevier; 2017;168:707–23.

49. Zhou F. Molecular Mechanisms of IFN-γ to Up-Regulate MHC Class I Antigen Processing and Presentation. Int Rev Immunol. 2009;28:239–60.

50. Berest I, Arnold C, Reyes-Palomares A, Palla G, Rasmussen KD, Giles H, et al. Quantification of Differential Transcription Factor Activity and Multiomics-Based Classification into Activators and Repressors: diffTF. Cell Rep. Elsevier; 2019;29:3147-3159.e12.

51. Belkahla S, Brualla JM, Fayd'herbe de Maudave A, Falvo P, Allende-Vega N, Constantinides M, et al. The metabolism of cells regulates their sensitivity to NK cells depending on p53 status. Sci Rep. 2022;12:3234.

52. Agresta L, Hoebe KHN, Janssen EM. The Emerging Role of CD244 Signaling in Immune Cells of the Tumor Microenvironment. Front Immunol [Internet]. Frontiers; 2018 [cited 2024 Sep 12];9. Available from: https://www.frontiersin.org/journals/immunology/articles/10.3389/fimmu.2018.02809/full

53. Ray A, Yuan C-Y, Miller NM, Mei H, Dittel BN. 2B4 Is Dispensable for T-Dependent B Cell Immune Responses, but Its Deficiency Leads to Enhanced T-Independent Responses Due to an Increase in Peritoneal Cavity B1b Cells. PLOS ONE. Public Library of Science; 2015;10:e0137314.

54. Brown DR, Calpe S, Keszei M, Wang N, McArdel S, Terhorst C, et al. Cutting Edge: An NK Cell-Independent Role for Slamf4 in Controlling Humoral Autoimmunity. J Immunol. 2011;187:21–5.

55. Shmerling M, Chalik M, Smorodinsky NI, Meeker A, Roy S, Sagi-Assif O, et al. LY6S, a New IFN-Inducible Human Member of the Ly6a Subfamily Expressed by Spleen Cells and Associated with Inflammation and Viral Resistance. ImmunoHorizons. 2022;6:253–72.

56. Acar A, Nichol D, Fernandez-Mateos J, Cresswell GD, Barozzi I, Hong SP, et al. Exploiting evolutionary steering to induce collateral drug sensitivity in cancer. Nat Commun. Nature Publishing Group; 2020;11:1923.

57. Umkehrer C, Holstein F, Formenti L, Jude J, Froussios K, Neumann T, et al. Isolating live cell clones from barcoded populations using CRISPRa-inducible reporters. Nat Biotechnol. 2021;39:174–8.

58. Baldwin LA, Bartonicek N, Yang J, Wu SZ, Deng N, Roden DL, et al. DNA barcoding reveals ongoing immunoediting of clonal cancer populations during metastatic progression and immunotherapy response. Nat Commun. Nature Publishing Group; 2022;13:6539.

59. Goyal Y, Busch GT, Pillai M, Li J, Boe RH, Grody EI, et al. Diverse clonal fates emerge upon drug treatment of homogeneous cancer cells. Nature. Nature Publishing Group; 2023;620:651–9.

60. Weinreb C, Rodriguez-Fraticelli A, Camargo FD, Klein AM. Lineage tracing on transcriptional landscapes links state to fate during differentiation. Science. 2020;367:eaaw3381.

61. Chang MT, Shanahan F, Nguyen TTT, Staben ST, Gazzard L, Yamazoe S, et al. Identifying transcriptional programs underlying cancer drug response with TraCe-seq. Nat Biotechnol. 2022;40:86–93.

62. Mittal D, Gubin MM, Schreiber RD, Smyth MJ. New insights into cancer immunoediting and its three component phases — elimination, equilibrium and escape. Curr Opin Immunol. NIH Public Access; 2014;27:16.

817 63. Ljunggren, H.G., Kärre, K. In serach of the “missing self”: MHC molecules and NK cell recognition.
818 Immunol Today. 1990;11:237–44.

819 64. Weichold FF, Jiang Y, Dunn DE, Bloom M, Malkovska V, Hensel NF, et al. Regulation of a Graft-
820 Versus-Leukemia Effect by Major Histocompatibility Complex Class II Molecules on Leukemia
821 Cells: HLA-DR1 Expression Renders K562 Cell Tumors Resistant to Adoptively Transferred
822 Lymphocytes in Severe Combined Immunodeficiency Mice/Nonobese Diabetic Mice. Blood.
823 1997;90:4553–8.

824 65. Xing S, Ferrari de Andrade L. NKG2D and MICA/B shedding: a ‘tag game’ between NK cells and
825 malignant cells. Clin Transl Immunol. 2020;9:e1230.

826 66. Konjević GM, Vuletić AM, Mirjačić Martinović KM, Larsen AK, Jurišić VB. The role of cytokines in
827 the regulation of NK cells in the tumor environment. Cytokine. 2019;117:30–40.

828 67. Holmes C, Stanford WL. Concise Review: Stem Cell Antigen-1: Expression, Function, and Enigma.
829 Stem Cells. 2007;25:1339–47.

830 68. Bradfute SB, Graubert TA, Goodell MA. Roles of Sca-1 in hematopoietic stem/progenitor cell
831 function. Exp Hematol. 2005;33:836–43.

832 69. Hordeaux J, Yuan Y, Clark PM, Wang Q, Martino RA, Sims JJ, et al. The GPI-Linked Protein LY6A
833 Drives AAV-PHP.B Transport across the Blood-Brain Barrier. Mol Ther. 2019;27:912–21.

834 70. Park JW, Park JM, Park DM, Kim D-Y, Kim HK. Stem Cells Antigen-1 Enriches for a Cancer Stem
835 Cell-Like Subpopulation in Mouse Gastric Cancer. Stem Cells. 2016;34:1177–87.

836 71. Li Y, Welm B, Podsypanina K, Huang S, Chamorro M, Zhang X, et al. Evidence that transgenes
837 encoding components of the Wnt signaling pathway preferentially induce mammary cancers
838 from progenitor cells. Proc Natl Acad Sci U S A. 2003;100:15853–8.

839 72. Roarty K, Baxley SE, Crowley MR, Frost AR, Serra R. Loss of TGF-β or Wnt5a results in an increase
840 in Wnt/β-catenin activity and redirects mammary tumour phenotype. Breast Cancer Res BCR.
841 2009;11:R19.

842 73. Batts TD, Machado HL, Zhang Y, Creighton CJ, Li Y, Rosen JM. Stem Cell Antigen-1 (Sca-1)
843 Regulates Mammary Tumor Development and Cell Migration. PLOS ONE. Public Library of
844 Science; 2011;6:e27841.

845 74. Liu D, Xu C, Liu Y, Ouyang W, Lin S, Xu A, et al. A systematic survey of LU domain-containing
846 proteins reveals a novel human gene, LY6A, which encodes the candidate ortholog of mouse Ly-
847 6A/Sca-1 and is aberrantly expressed in pituitary tumors. Front Med [Internet]. 2023 [cited 2023
848 Jul 18]; Available from: https://link.springer.com/10.1007/s11684-022-0968-4

849 75. Luo L, McGarvey P, Madhavan S, Kumar R, Gusev Y, Upadhyay G. Distinct lymphocyte antigens 6
850 (Ly6) family members Ly6D, Ly6E, Ly6K and Ly6H drive tumorigenesis and clinical outcome.
851 Oncotarget. 2016;7:11165–93.

852 76. Zhao J, Jin D, Huang M, Ji J, Xu X, Wang F, et al. Glycolysis in the tumor microenvironment: a
853 driver of cancer progression and a promising therapeutic target. Front Cell Dev Biol [Internet].
854 Frontiers; 2024 [cited 2024 Sep 18];12. Available from:
855 https://www.frontiersin.org/journals/cell-and-developmental-
856 biology/articles/10.3389/fcell.2024.1416472/full

857 77. Pflugh DL, Maher SE, Bothwell ALM. Ly-6 superfamily members Ly-6A/E, Ly-6C, and Ly-6I
858 recognize two potential ligands expressed by B lymphocytes. J Immunol Baltim Md 1950.
859 2002;169:5130–6.

860 78. Shokouhifar A, Firouzi J, Nouri M, Sarab GA, Ebrahimi M. NK cell upraise in the dark world of
861 cancer stem cells. Cancer Cell Int. 2021;21:682.

862 79. Tsuchiya H, Shiota G. Immune evasion by cancer stem cells. Regen Ther. 2021;17:20–33.

863 80. ClustVis: a web tool for visualizing clustering of multivariate data using Principal Component
864 Analysis and heatmap | Nucleic Acids Research | Oxford Academic [Internet]. [cited 2023 Feb
865 21]. Available from: https://academic.oup.com/nar/article/43/W1/W566/2467929

866

867 # Figure legends

868 **Figure 1: Co-culture system to study cancer immunoediting *in vitro*. (A)** Scheme illustrates the
869 experimental setup: BCR/ABL^{p185+} B-ALL leukaemic cells (LCs) are transduced with a DNA barcode
870 library. Barcoded LCs are co-cultured with NK cells for 4-20 days *in vitro*. **(B)** Ten B-ALL cell lines were
871 generated from C57BL/6 WT mice and characterised regarding the surface expression of NK cell
872 receptor ligands (black) and their susceptibility towards NK cell killing (red, depicted here is the
873 cytotoxicity at E:T=10:1) measured by flow cytometry. Cell lines #13 and #15, in blue, showed the
874 highest NK cell susceptibility and were used for the following experiments. Rows were centred; unit
875 variance scaling was applied to rows. Both rows and columns were clustered using correlation distance
876 and average linkage. The plot was generated using the Clustvis web tool (80). **(C)** B-ALL cell lines were
877 DNA barcoded by lentiviral transduction. Using different amounts of viral supernatant, the optimum
878 transduction efficiency of <5% GFP^{+} cells (18) was chosen to allow a single barcode integration per cell.
879 Shown are means±SD (n=2) of one representative cell line. **(D)** Two B-ALL cell lines (#13 and #15) were
880 barcoded and the barcode diversity of the FACS-purified GFP^{+} cell lines was determined by targeted
881 DNA sequencing. Cell lines A and B were derived from #13 and cell lines C and D from #15. Bars show
882 barcode diversity of barcoded tumour cell lines (A&D n=3 and B&C n=2 independent experiments, each
883 determined by sequencing of 3 biological and 2 technical replicates). Shown is median with
884 interquartile range. **(E)** Barcoded WT B-ALL cell lines A-D were cultivated in three individual wells either
885 in the absence or presence of purified and IL-2-activated NK cells. One *B2m*$^{-/-}$ B-ALL cell line was
886 included as control. Absolute numbers of B-ALL cells were determined by flow cytometry. On day 0, 4
887 and 14, B-ALL cells were FACS sorted, re-plated and fresh NK cells were replenished. Shown are
888 means±SD of n=4 B-ALL cell lines of one representative experiment (n=3 independent experiments);
889 the significance was calculated by an unpaired t-test on day 4, 14 and 20. **(F)** On day 29, a 4 hour NK
890 cytotoxicity assay was performed using B-ALL cells that had been cultured for 20 days in the presence
891 or absence of NK cells. Shown are means±SD of n=4 cell lines (in technical triplicates) of one
892 representative experiment (n=3 experiments); the significance was calculated by a paired t-test.

893 **Figure 2: Quantification of NK cell-mediated cancer immunoediting *in vitro*. (A)** Schematic
894 representation of the proposed model. Scheme was created in BioRender. Kovar, H. (2023)
895 BioRender.com/j11m245. **(B)** Upon long-term co-culture of B-ALL and NK cells, we hypothesised that
896 each tumour cell clone would fall into one of the following categories: The abundance of a clone can
897 be significantly higher (primary resistant) or lower (eliminated), unchanged (static) or show a high
898 variability (secondary resistant) upon NK cell co-culture. Variability is defined as $v = log2(max(x +$
899 $1)/min(x + 1))$, where x is a vector of normalised counts across samples. A rule-based decision tree
900 was designed to discriminate the four categories depicted in (A). **(C)** The percentage of the cell clones
901 in each group on day 14 is depicted for cell lines A, B, C and D. Each data point represents the mean
902 value (n=3 wells, sequenced in duplicates) of n=2-3 independent experiments. **(D)** The heatmap shows
903 the normalised abundance of barcodes (norm. BC abundance) of cell line A from one representative
904 experiment. Each subcolumn (n=3) in the figure represents a sample (well), and each row represents
905 a barcode. The barcodes were divided into the four pre-defined groups according to the criteria
906 defined in (B). The Shannon diversity index (shown above the heatmap) serves as measure of barcode
907 diversity and drops significantly after 14 days of NK co-culture. The histogram on the left shows the
908 average abundance of the barcoded cell clone in the B-ALL only samples on day 4. **(E)** The bubble plot
909 depicts the normalised abundance of secondary resistant clones in B-ALL samples (day 4) compared to
910 B-ALL + NK samples (day 14). The x-axis shows the three individual wells of each condition, while each
911 row on the y-axis shows an individual tumour cell clone. The size and colour of the bubbles indicate
912 the normalised barcode abundance. Shown is the same cell line and experiment as in (D). **(F)**
913 Comparing two independent experiments in cell line A as shown in (D&E), the Euler diagrams highlight
914 a high overlap of eliminated, primary resistant, and static cell clones. In contrast, only two secondary
915 resistant clones were shared between both independent experiments.
916
917 **Figure 3: Integrative analysis of RNA and ATAC sequencing shows well-known and novel genes**
918 **deregulated in NK cell resistant B-ALL cells.** The **(A-D and G)** transcriptome and **(E-I)** chromatin
919 accessibility analysis of B-ALL cells co-cultured with NK cells for 4 (time point 1 (TP1)) or 14 (TP2) days

920 were analysed and compared to the B-ALL alone cells on TP1 (n=3-4 independent experiments). **(A)**
921 The volcano plot shows the significantly up- or downregulated genes in B-ALL cell lines A and B after
922 co-culture with NK cells for 14 days (n=3 experiments). Statistics were calculated with the Wald test.
923 **(B)** The dot plot illustrates the enrichment analysis using the hyperR tool (31) for the Gene Ontology
924 Biological Process (GOBP) terms associated with NK cell co-cultured B-ALL cells shown in panel (A). X-
925 axis and dot colour depicts the false discovery rate (FDR) and y-axis the corresponding biological
926 processes. Dot size illustrates the number of genes associated with the biological processes. **(C)** The
927 Euler diagrams display up- or downregulated genes in cell lines A/B and/or C/D after 14 days of NK cell
928 co-culture. **(D)** The heatmap shows the expression of selected overlapping genes (top-20 upregulated,
929 top-10 downregulated; ranked by p-value) identified in (C) (n=3-4 experiments, 4 B-ALL cell lines). The
930 row-scaled normalised counts represent the $\log_2$(fold change). **(E)** The volcano plot shows DARs in B-
931 ALL cells A/B after co-culture with NK cells for 14 days (n=3 experiments). Statistics were calculated
932 with the Wald test. **(F)** The Euler diagrams highlight genes whose promoters (TSS ± 3kb) had higher or
933 lower chromatin accessibility in cell lines A/B and/or C/D after 14 days of NK cell co-culture in n=3-4
934 experiments. Gene promoters with the highest $\log_2$(fold change) are highlighted. **(G)** Integration of
935 RNA and ATAC sequencing data shows that 37 genes are up- and 16 downregulated in cell lines A/B;
936 the top 10 up- or downregulated genes are highlighted on the right. **(H)** Analysis of differential
937 transcription factors activity using (diffTF) (41) highlighted activator (green) and repressor (red) TFs
938 that were differentially expressed in B-ALL cell lines A/B after NK cell co-culture. **(I)** Integrative
939 Genomics Viewer (IGV) genome browser tracks display representative ATAC sequencing signal
940 densities at the *Ly6a* and *Plaat3* loci in B-ALL cells with or without NK cell co-culture. Shown are the
941 gene bodies including a 3 kb upstream promoter region, as well as binding sites of TFs identified in (H).
942 Database HOCOMOCO (v10) (42) was used and depicted are counts per million (CPM) with a range of
943 [0-1.37].
944
945 **Figure 4: The combination of NK cell cytotoxicity and IFN-γ production drives tumour**
946 **immunoediting. (A&C)** Barcoded B-ALL cell lines (n=2 cell lines A/D) were cultivated in three individual

947 wells either in the absence or presence of purified and IL-2-activated WT, **(A)** *Prf1*$^{-/-}$ or **(C)** *Ifng*$^{-/-}$ NK
948 cells. Absolute numbers of B-ALL cells were determined by flow cytometry. On day 0, 4 and 14/17 B-
949 ALL cells were FACS sorted, re-plated and fresh NK cells were replenished. **(A)** Shown are means±SD of
950 n=2 cell lines. The significance was calculated with the Kruskal-Wallis test and Dunn´s multiple
951 comparisons testing. **(B&D)** On the last day of the NK cell co-culture experiment, a standard 4 hour NK
952 cytotoxicity assay with WT NK cells was performed using B-ALL cells that had been cultured for 4 weeks
953 in the presence or absence of NK cells. Shown are means±SD of technical triplicates. Statistics were
954 calculated for the highest E:T ratio with one-way ANOVA with Tukey´s multiple comparisons test.
955 **(E&G)** The Shannon diversity of leukaemic clones dropped significantly (*p=0.0219*) upon co-culture
956 with WT NK cells, and to a lesser degree with **(E)** *Prf1*$^{-/-}$ or **(G)** *Ifng*$^{-/-}$ NK cells. Shown is the mean and
957 dots depict each replicate. Statistics were calculated with the Kruskal-Wallis and Dunn´s multiple
958 comparisons testing. **(F&H)** The barcodes within each sample were classified according to the decision
959 tree in Fig. 2B. The barcodes that were attributed to the four pre-defined groups were compared
960 between the treatment groups with Euler diagrams for each group [eliminated, resistant (1st), resistant
961 (2nd) and static]. **(I&J)** The Euler diagrams display the number of up- and downregulated genes in cell
962 lines A/D after 14 days of co-culture with WT or *Prf1*$^{-/-}$ NK cells. Top 10 up- or downregulated genes in
963 the intersection or specific for WT or *Prf1*$^{-/-}$ NK cell co-culture are depicted in the corresponding lists.
964 **(K)** The volcano plot depicts DEGs in B-ALL + WT NK *versus* B-ALL + *Ifng*$^{-/-}$ NK conditions on day 17 of
965 cell line A. **(L)** The Euler diagram depicts DEGs when comparing B-ALL + WT or B-ALL + *Ifng*$^{-/-}$ NK
966 conditions with B-ALL alone. Top 10 WT NK cell specific genes and the overlapping genes are depicted
967 in the corresponding lists. Shown is **(A, B, I, J)** one experiment including n=2 cell lines A/D or **(C-H, K,**
968 **L)** one experiment from cell line A. Data is representative for two independent experiments and n=2
969 cell lines.
970
971 **Figure 5: The role of mouse Ly6A in the evasion of leukaemic cells from NK cell-mediated**
972 **surveillance. (A)** The bar graph shows the protein abundance of Ly6A on day 14 of the same co-culture
973 experiments as described in Figure 4A. Two B-ALL cell lines (A in circles/D in triangles) were analysed

974 by mass spectrometry in triplicates. Bars and error bars represent means of arbitrary units (AU) relative
975 to the whole protein abundance ±SD; the significance was calculated by one-way ANOVA with Tukey´s
976 multiple comparisons test. **(B)** Ly6A surface expression was measured on B-ALL cells co-cultured with
977 WT or *Ifng*$^{-/-}$ NK cells for 17/18 or 32/30 days. Bars represent means (n=3-4 for cell line D from two
978 independent experiments). **(C)** *Ly6a* KO clones were generated by CRISPR/Cas9 genome editing in
979 parental B-ALL cell lines. The gene modification was verified by measuring Ly6A surface expression by
980 flow cytometry. Histogram shows the Ly6A expression in one representative *Ly6a* WT and KO clone.
981 **(D)** Growth curve of *Ly6a* WT and KO B-ALL clones in absolute cell numbers over 13 days. Shown are
982 means±SD of n=2 cell lines per genotype, measured in technical duplicates. **(E)** Cell viability of *Ly6a* WT
983 and KO B-ALL clones. Shown are means±SD of n=2 clones per genotype of n=3 independent
984 experiments. **(F)** The volcano plot shows DEGs (n=342) of *Ly6a* WT and KO clones (n=2 clones per
985 genotype, sequenced in technical triplicates) under normal culturing conditions. Differentially up- or
986 downregulated genes are depicted in red and blue, respectively. **(G)** The dot plot illustrates the GOBP
987 terms associated with *Ly6a*-deficiency in B-ALL cells shown in panel (F). X-axis and dot colour depicts
988 the false discovery rate (FDR) and y-axis the corresponding biological processes. Dot size illustrates the
989 number of genes associated with the biological processes. **(H)** An ATP rate assay was performed in
990 *Ly6a* WT and KO cells. Bar graph depicts means±SD of mitochondrial and glycolytic ATP production;
991 the significance was calculated by an unpaired t-test. **(I)** *Ly6a* WT and KO B-ALL cell lines (n=4 per
992 genotype) were characterised by their surface expression of NK cell receptor ligands by flow cytometry.
993 Columns represent different tumour cell clones ordered according to genotype and cell line. Data has
994 been scaled and clustered by row to highlight variations in marker expression across different
995 samples. Red indicates higher and blue lower expression levels of surface ligands. **(J)** The expression
996 of CD244 on the surface of WT and *Ly6a* KO clones was determined by flow cytometry. The bars and
997 error bars represent the mean±SD of the MFIs of n=2 clones per genotype and two independent
998 experiments. Statistics were calculated using an unpaired t-test. **(K)** Measurement of IFN-γ^{+} mNK cells
999 upon co-culture with *Ly6a* WT and KO B-ALL cell lines for 4 hours (n=2 clones per genotype and
1000 technical triplicates). As positive control mNK cells were activated with IL-12/15/18. **(L)** Measurements

1001 of MFI of granzyme B in freshly isolated NK cells co-cultured with *Ly6a* WT and KO clones for 4 hours.
1002 Shown are means±SD of n=2 clones per genotype and two independent experiments. **(M)** *Ly6a* WT and
1003 KO B-ALL cell lines were co-incubated with WT NK cells for 10 min before the flow cytometric-based
1004 assessment of tumour-NK conjugate formation (n=6 clones per genotype). **(N)** A 4 hour NK cytotoxicity
1005 assay was performed using WT and *Ly6a* KO B-ALL clones. Shown are means±SD of n=2 clones per
1006 genotype and 3 independent experiments; statistics were calculated using an unpaired t-test.

1007

1008 **Figure 6: The role of human LY6E in the evasion of leukaemic cells from NK cell-mediated**
1009 **surveillance. (A)** Kaplan-Meier plot depicts survival probabilities of the TARGET-ALL-P2 patient cohort
1010 divided into *LY6E* high and low expressing groups (cut-off percentile = 60%). Graph was generated by
1011 using the online web tool: cSurvival (ubc.ca). **(B)** *LY6E* WT and KO K562 clones were analysed for their
1012 expression of LY6E in the absence or presence of IFN-β (upper panel) or IFN-γ (lower panel) by Western
1013 blotting. β-actin served as loading control. **(C)** The volcano plot shows DEGs (n=829) of *LY6E* WT and
1014 KO K562 clones under normal culturing conditions (n=2 clones per genotype, sequenced in technical
1015 triplicates). Differentially up- or downregulated genes are depicted in red and blue, respectively. **(D)**
1016 The dot plot illustrates the GOBP terms associated with *LY6E*-deficiency in K562 cells shown in panel
1017 (C). X-axis and dot colour depicts the false discovery rate (FDR) and y-axis the corresponding biological
1018 processes. Dot size illustrates the number of genes associated with the biological processes. **(E)** Growth
1019 curve of *LY6E* WT and KO K562 clones in absolute cell numbers over 14 days. Shown is one cell line per
1020 genotype, representative of two cell lines. **(F)** Cell viability of *LY6E* WT and KO K562 clones. Shown are
1021 means±SD of n=2 cell lines per genotype and 3 independent experiments. **(G)** A 1 hour NK cytotoxicity
1022 assay was performed using WT and *LY6E* KO K562 clones. Shown are means±SD of n=2 clones per
1023 genotype and 2 independent experiments. Statistics were calculated using an unpaired t-test. **(H)** *LY6E*
1024 WT and KO cell clones were co-incubated with NK cells and the tumour-NK cell conjugate formation
1025 was assessed by flow cytometry. Bars and error bars represent means±SD of n=2 clones per genotype
1026 and 4 independent experiments. Statistics were calculated using an unpaired t-test.

1027 ## Acknowledgements

1028 We thank Veronika Sexl (VetMedUni Vienna, Austria) for providing the BCR/ABL^{p185} construct, Thomas
1029 Kolbe (VetMedUni Vienna, Austria) for providing the *B2m*$^{-/-}$ mice and Sabine Strehl and Klaus
1030 Fortschegger (CCRI, Austria) for discussions and sharing information. We are grateful to Marcus Toetzl
1031 for assistance with ATAC-seq library preparation and Melanie Hofmann and Gernot Schabbauer for
1032 support with the Seahorse experiments. We thank the CCRI FACS and Bioinformatics Core Units for
1033 assistance with cell sorting and bioinformatics/statistics, respectively, the Core Facility Laboratory
1034 Animal Breeding and Husbandry of the Medical University of Vienna (MUW, Austria) for taking care of
1035 our mice and the Biomedical Sequencing Facility and the Proteomics Facility of the CeMM Research
1036 Centre for Molecular Medicine of the Austrian Academy of Sciences for their support on next-
1037 generation sequencing and mass spectrometry analysis, respectively. This work was supported by the
1038 St. Anna Children's Cancer Research Institute (Vienna, Austria), by a DOC fellowship of the Austrian
1039 Academy of Sciences awarded to M.C.B. (#25905), and by grants from the Fellinger Krebsforschung to
1040 E.M.P. and from the Austrian Science Fund (10.55776/P32001-B, 10.55776/P34832 and
1041 10.55776/WKP132-B to E.M.P.; 10.55776/TAI 454 and 10.55776/TAI 732 to F.H.; 10.55776/P31563 and
1042 10.55776/I4649 to X.K.). F.H. was supported by funding from the Alex's Lemonade Stand Foundation
1043 for Childhood Cancer (20-17258) and A.R.P. was supported by the Mildred Scheel Early Career Center
1044 Dresden P2, funded by the German Cancer Aid.

1045 ## Author contributions

1046 Conceptualisation: E.M.P.

1047 Methodology: M.C.B., B.K., E.M.P., with input from J.U., J.C., L.P., T.S., D.G.,

1048 Formal analysis: M.C.B., M.R.S, A.B., P.R., D.S., A.R.P., E.M.P.

1049 Investigation: M.C.B., H.B., A.D., F.O.D., B.K., F.H.-G., S.D., L.S., S.S., D.E., D.G.

1050 Writing (original draft): M.C.B., E.M.P.

1051 Visualisation: M.C.B., M.R.S., A.B., X.K., E.M.P.

1052 Resources: J.U., J.C., M.L., L.P., T.S., F.H., E.M.P.

1053 Supervision: F.H., E.M.P.

1054 Funding acquisition: M.C.B., E.M.P.

1055 All authors reviewed and edited the manuscript.

1056 Additional information

1057 **Corresponding author:** Eva Maria Putz, Center for Physiology and Pharmacology, Institute of

1058 Pharmacology, Medical University of Vienna, Waehringer Strasse 13A, 1090 Vienna, Austria. E-mail:

1059 eva-maria.putz@meduniwien.ac.at

Figure 1

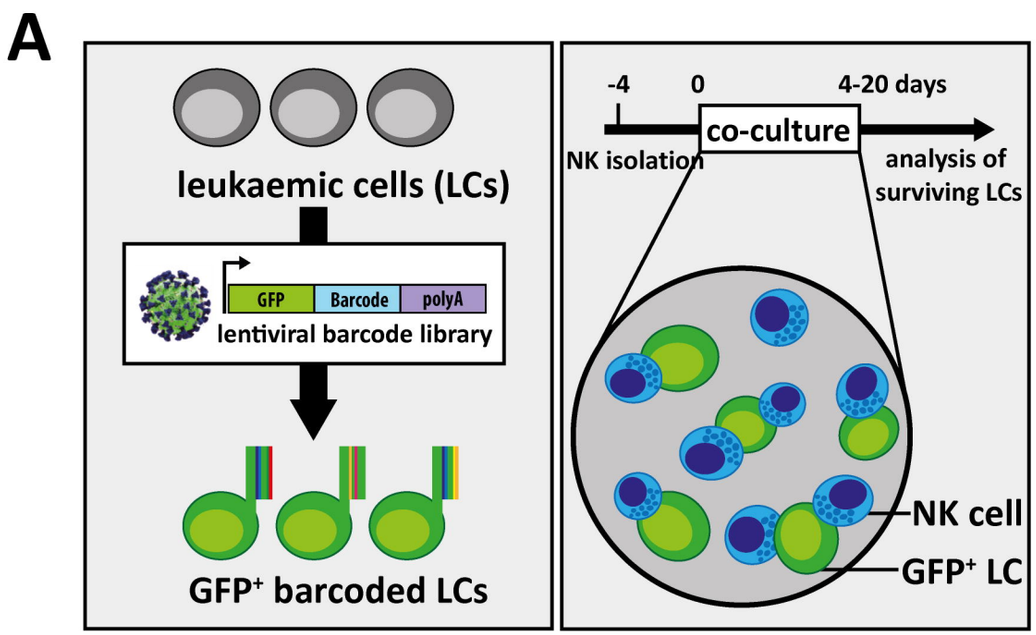
A
leukaemic cells (LCs)
GFP
Barcode
polyA
lentiviral barcode library
GFP+ barcoded LCs
-4
0
4-20 days
co-culture
NK isolation
analysis of surviving LCs
NK cell
GFP+ LC

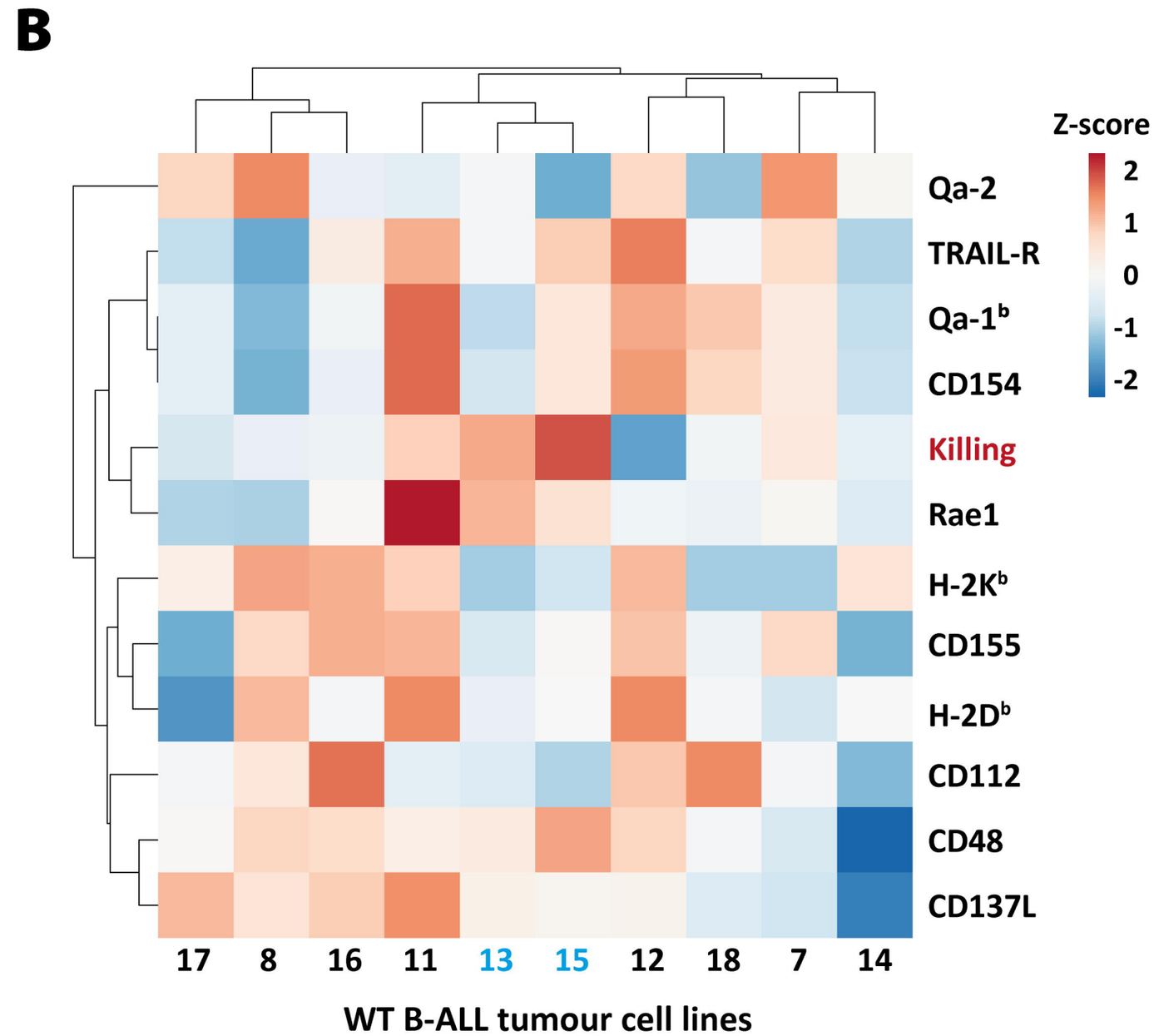
B
Z-score
2
1
0
-1
-2
Qa-2
TRAIL-R
Qa-1b
CD154
Killing
Rae1
H-2Kb
CD155
H-2Db
CD112
CD48
CD137L
17
8
16
11
13
15
12
18
7
14
WT B-ALL tumour cell lines

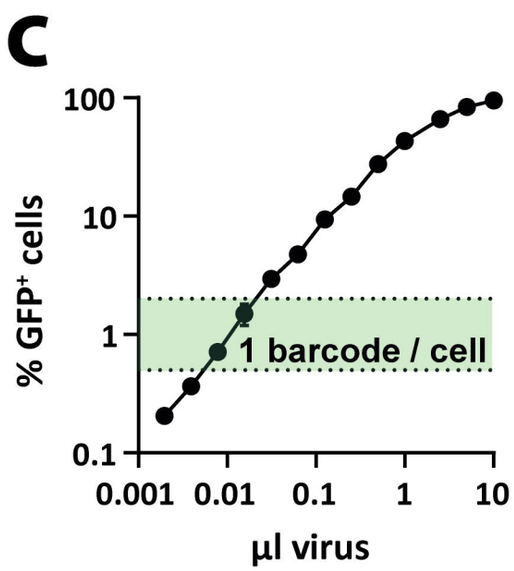
C
% GFP+ cells
100
10
1
0.1
1 barcode / cell
0.001
0.01
0.1
1
10
µl virus

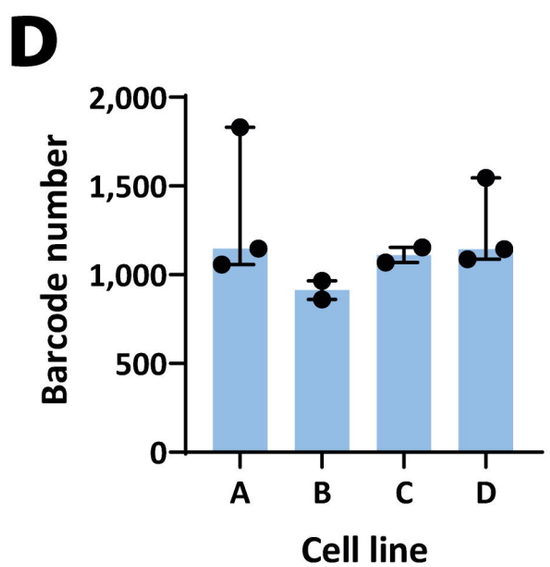
D
Barcode number
2,000
1,500
1,000
500
0
A
B
C
D
Cell line

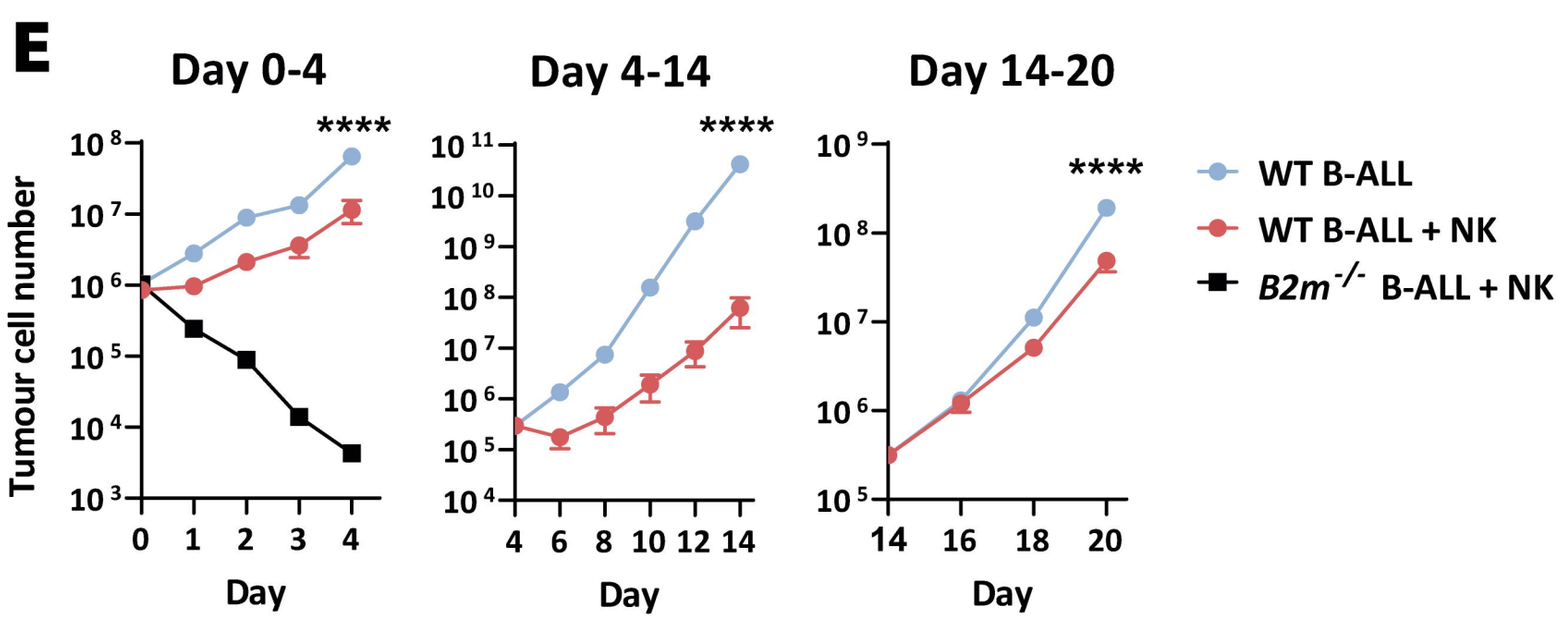
E
Day 0-4
Day 4-14
Day 14-20
****
Tumour cell number
Day
WT B-ALL
WT B-ALL + NK
B2m-/- B-ALL + NK

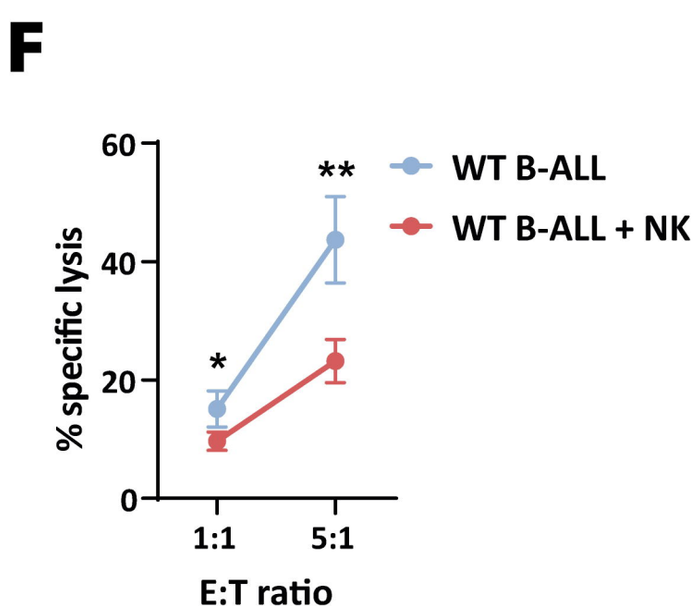
F
% specific lysis
60
40
20
0
*
**
1:1
5:1
E:T ratio
WT B-ALL
WT B-ALL + NK

Figure 2

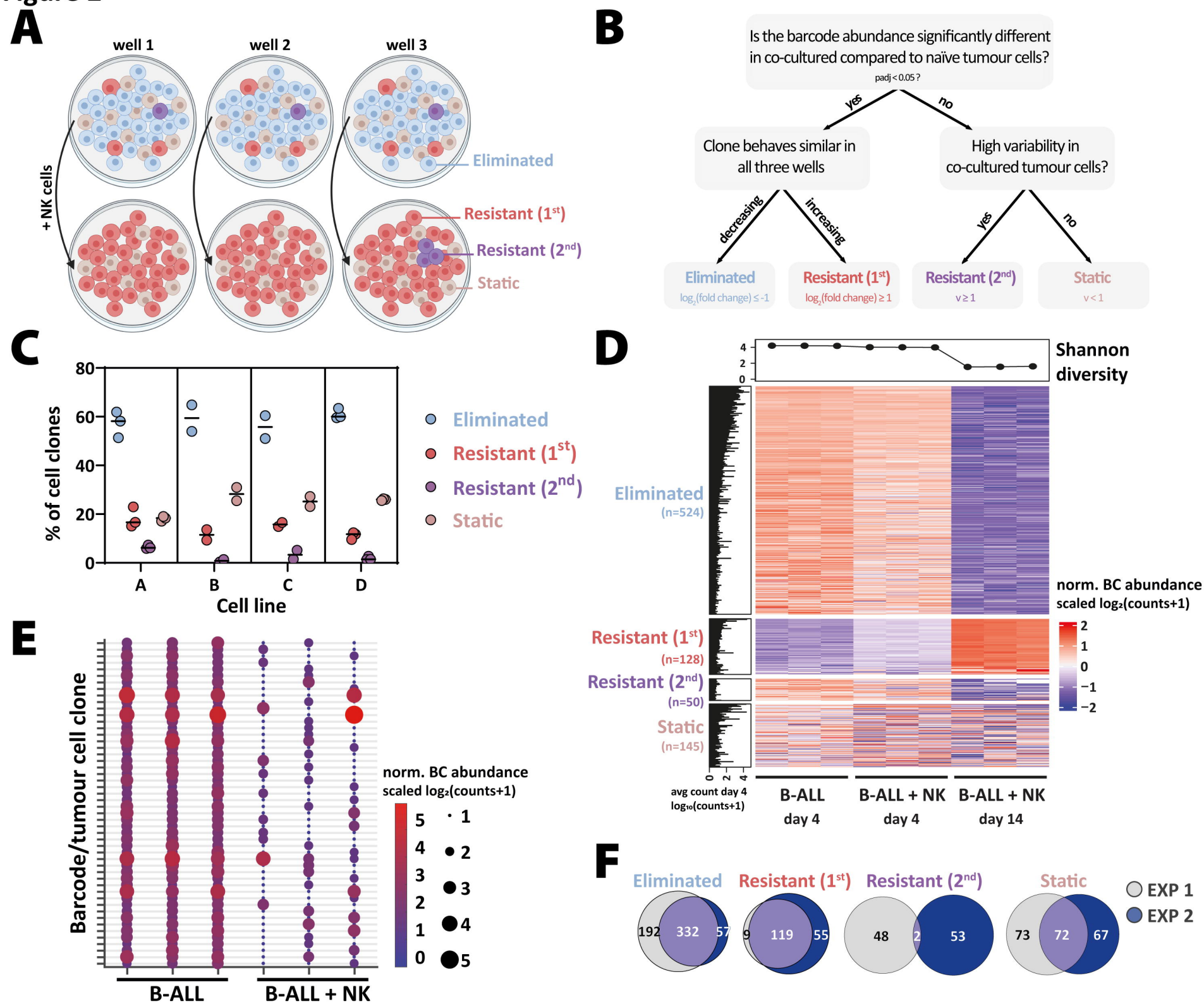
A
well 1
well 2
well 3
+ NK cells
Eliminated
Resistant (1st)
Resistant (2nd)
Static
B
Is the barcode abundance significantly different in co-cultured compared to naïve tumour cells?
padj < 0.05 ?
yes
no
Clone behaves similar in all three wells
High variability in co-cultured tumour cells?
decreasing
increasing
yes
no
Eliminated
log2(fold change) ≤ -1
Resistant (1st)
log2(fold change) ≥ 1
Resistant (2nd)
v ≥ 1
Static
v < 1
C
% of cell clones
80
60
40
20
0
A
B
C
D
Cell line
Eliminated
Resistant (1st)
Resistant (2nd)
Static
D
Shannon diversity
4
2
0
Eliminated
(n=524)
Resistant (1st)
(n=128)
Resistant (2nd)
(n=50)
Static
(n=145)
norm. BC abundance
scaled log2(counts+1)
2
1
0
−1
−2
avg count day 4
log10(counts+1)
B-ALL
day 4
B-ALL + NK
day 4
B-ALL + NK
day 14
E
Barcode/tumour cell clone
norm. BC abundance
scaled log2(counts+1)
5
4
3
2
1
0
1
2
3
4
5
B-ALL
B-ALL + NK
F
Eliminated
192
332
57
Resistant (1st)
9
119
55
Resistant (2nd)
48
2
53
Static
73
72
67
EXP 1
EXP 2

Figure 3

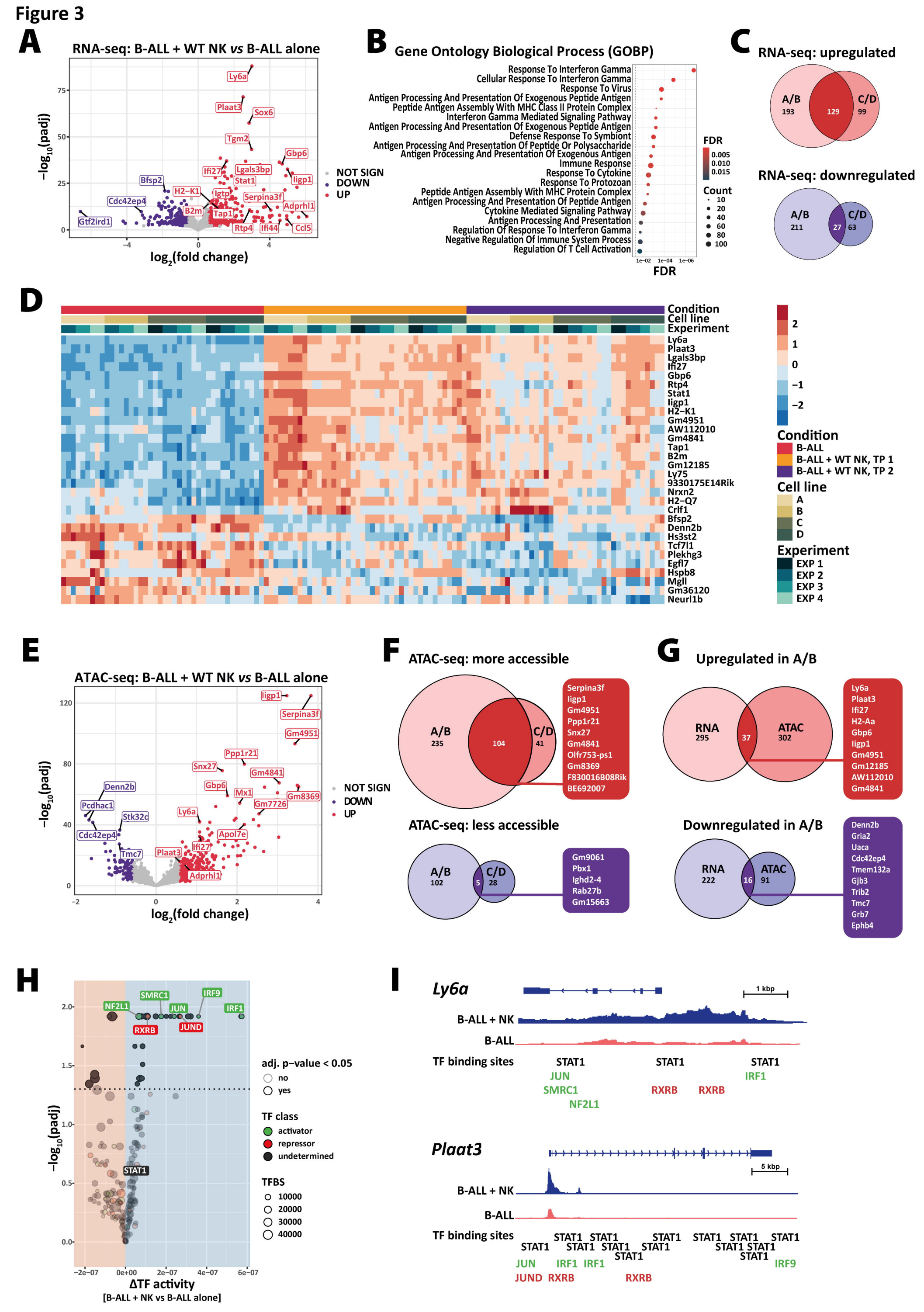
A
RNA-seq: B-ALL + WT NK vs B-ALL alone
−log10(padj)
log2(fold change)
NOT SIGN
DOWN
UP
Ly6a
Plaat3
Sox6
Tgm2
Gbp6
Ifi27
Lgals3bp
Stat1
Iigp1
Bfsp2
H2−K1
Igtp
Serpina3f
Cdc42ep4
B2m
Tap1
Adprhl1
Gtf2ird1
Rtp4
Ifi44
Ccl5
B
Gene Ontology Biological Process (GOBP)
Response To Interferon Gamma
Cellular Response To Interferon Gamma
Response To Virus
Antigen Processing And Presentation Of Exogenous Peptide Antigen
Peptide Antigen Assembly With MHC Class II Protein Complex
Interferon Gamma Mediated Signaling Pathway
Antigen Processing And Presentation Of Exogenous Peptide Antigen
Defense Response To Symbiont
Antigen Processing And Presentation Of Peptide Or Polysaccharide
Antigen Processing And Presentation Of Exogenous Antigen
Immune Response
Response To Cytokine
Response To Protozoan
Peptide Antigen Assembly With MHC Protein Complex
Antigen Processing And Presentation Of Peptide Antigen
Cytokine Mediated Signaling Pathway
Antigen Processing And Presentation
Regulation Of Response To Interferon Gamma
Negative Regulation Of Immune System Process
Regulation Of T Cell Activation
FDR
Count
C
RNA-seq: upregulated
A/B 193
129
C/D 99
RNA-seq: downregulated
A/B 211
27
C/D 63
D
Condition
Cell line
Experiment
Ly6a
Plaat3
Lgals3bp
Ifi27
Gbp6
Rtp4
Stat1
Iigp1
H2−K1
Gm4951
AW112010
Gm4841
Tap1
B2m
Gm12185
Ly75
9330175E14Rik
Nrxn2
H2−Q7
Crlf1
Bfsp2
Denn2b
Hs3st2
Tcf7l1
Plekhg3
Egfl7
Hspb8
Mgll
Gm36120
Neurl1b
B-ALL
B-ALL + WT NK, TP 1
B-ALL + WT NK, TP 2
A
B
C
D
EXP 1
EXP 2
EXP 3
EXP 4
E
ATAC-seq: B-ALL + WT NK vs B-ALL alone
−log10(padj)
log2(fold change)
NOT SIGN
DOWN
UP
Iigp1
Serpina3f
Gm4951
Ppp1r21
Snx27
Gm4841
Gbp6
Mx1
Gm8369
Gm7726
Denn2b
Pcdhac1
Stk32c
Ly6a
Cdc42ep4
Apol7e
Tmc7
Plaat3
Ifi27
Adprhl1
F
ATAC-seq: more accessible
A/B 235
104
C/D 41
Serpina3f
Iigp1
Gm4951
Ppp1r21
Snx27
Gm4841
Olfr753-ps1
Gm8369
F830016B08Rik
BE692007
ATAC-seq: less accessible
A/B 102
5
C/D 28
Gm9061
Pbx1
Ighd2-4
Rab27b
Gm15663
G
Upregulated in A/B
RNA 295
37
ATAC 302
Ly6a
Plaat3
Ifi27
H2-Aa
Gbp6
Iigp1
Gm4951
Gm12185
AW112010
Gm4841
Downregulated in A/B
RNA 222
16
ATAC 91
Denn2b
Gria2
Uaca
Cdc42ep4
Tmem132a
Gjb3
Trib2
Tmc7
Grb7
Ephb4
H
NF2L1
SMRC1
JUN
IRF9
IRF1
RXRB
JUND
STAT1
−log10(padj)
ΔTF activity
[B-ALL + NK vs B-ALL alone]
adj. p−value < 0.05
no
yes
TF class
activator
repressor
undetermined
TFBS
10000
20000
30000
40000
I
Ly6a
1 kbp
B-ALL + NK
B-ALL
TF binding sites
STAT1
JUN
SMRC1
NF2L1
RXRB
IRF1
Plaat3
5 kbp
JUND
IRF9

Figure 4

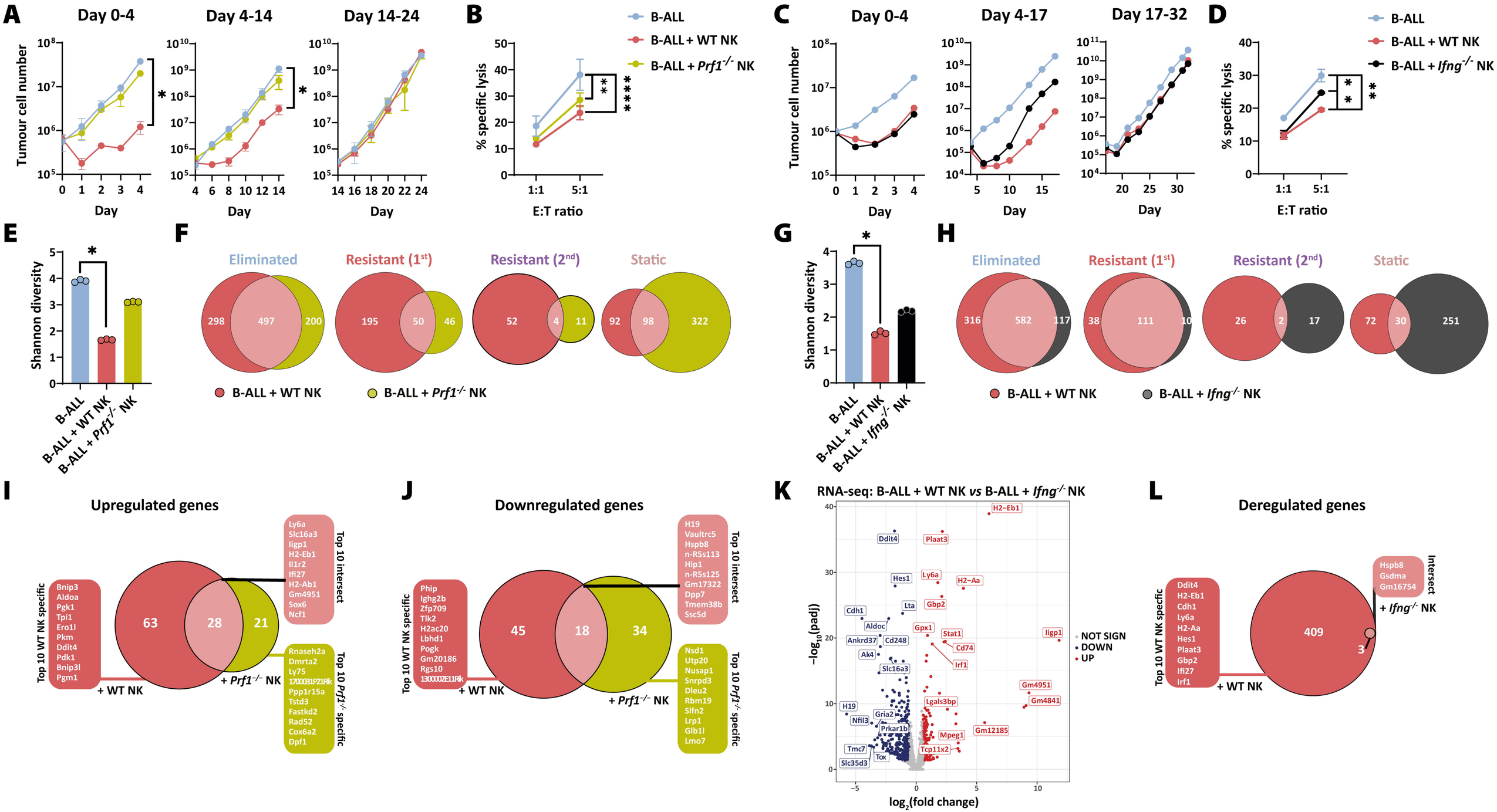
A
Day 0-4
Day 4-14
Day 14-24
Tumour cell number
Day
B
B-ALL
B-ALL + WT NK
B-ALL + Prf1-/- NK
% specific lysis
E:T ratio
C
Day 0-4
Day 4-17
Day 17-32
D
B-ALL + Ifng-/- NK
E
Shannon diversity
F
Eliminated
Resistant (1st)
Resistant (2nd)
Static
298 497 200
195 50 46
52 4 11
92 98 322
G
H
316 582 117
38 111 10
26 2 17
72 30 251
I
Upregulated genes
Top 10 WT NK specific
Bnip3 Aldoa Pgk1 Tpi1 Ero1l Pkm Ddit4 Pdk1 Bnip3l Pgm1
63 28 21
Top 10 intersect
Ly6a Slc16a3 Iigp1 H2-Eb1 Il1r2 Ifi27 H2-Ab1 Gm4951 Sox6 Ncf1
Top 10 Prf1-/- specific
Rnaseh2a Dmrta2 Ly75 1700031P21Rik Ppp1r15a Tstd3 Fastkd2 Rad52 Cox6a2 Dpf1
+ WT NK
+ Prf1-/- NK
J
Downregulated genes
Phip Ighg2b Zfp709 Tlk2 H2ac20 Lbhd1 Pogk Gm20186 Rgs10 1300002E11Rik
45 18 34
H19 Vaultrc5 Hspb8 n-R5s113 Hip1 n-R5s125 Gm17322 Dpp7 Tmem38b Ssc5d
Nsd1 Utp20 Nusap1 Snrpd3 Dleu2 Rbm19 Slfn2 Lrp1 Glb1l Lmo7
K
RNA-seq: B-ALL + WT NK vs B-ALL + Ifng-/- NK
−log10(padj)
log2(fold change)
NOT SIGN
DOWN
UP
H2-Eb1 Ddit4 Plaat3 Hes1 Ly6a H2-Aa Lta Gbp2 Cdh1 Aldoc Gpx1 Stat1 Iigp1 Ankrd37 Cd248 Cd74 Ak4 Irf1 Slc16a3 Gm4951 Gm4841 Lgals3bp H19 Gria2 Nfil3 Prkar1b Gm12185 Mpeg1 Tmc7 Tcp11x2 Tox Slc35d3
L
Deregulated genes
Intersect
Hspb8 Gsdma Gm16754
Top 10 WT NK specific
Ddit4 H2-Eb1 Cdh1 Ly6a H2-Aa Hes1 Plaat3 Gbp2 Ifi27 Irf1
409 3
+ WT NK
+ Ifng-/- NK

Figure 5

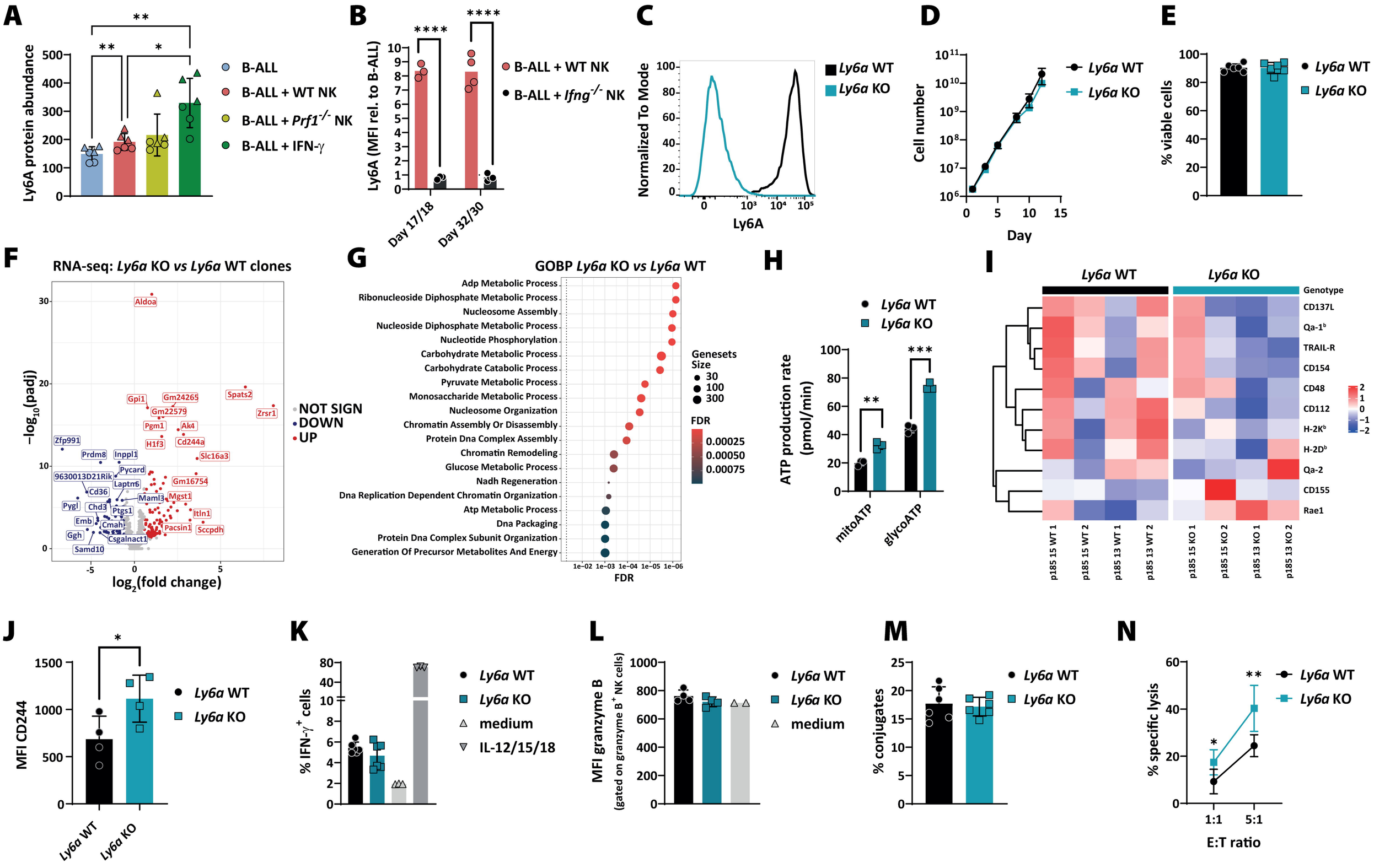
A
Ly6A protein abundance
B-ALL
B-ALL + WT NK
B-ALL + Prf1-/- NK
B-ALL + IFN-γ
B
Ly6A (MFI rel. to B-ALL)
B-ALL + WT NK
B-ALL + Ifng-/- NK
Day 17/18
Day 32/30
C
Normalized To Mode
Ly6A
Ly6a WT
Ly6a KO
D
Cell number
Day
Ly6a WT
Ly6a KO
E
% viable cells
Ly6a WT
Ly6a KO
F
RNA-seq: Ly6a KO vs Ly6a WT clones
−log10(padj)
log2(fold change)
NOT SIGN
DOWN
UP
G
GOBP Ly6a KO vs Ly6a WT
Adp Metabolic Process
Ribonucleoside Diphosphate Metabolic Process
Nucleosome Assembly
Nucleoside Diphosphate Metabolic Process
Nucleotide Phosphorylation
Carbohydrate Metabolic Process
Carbohydrate Catabolic Process
Pyruvate Metabolic Process
Monosaccharide Metabolic Process
Nucleosome Organization
Chromatin Assembly Or Disassembly
Protein Dna Complex Assembly
Chromatin Remodeling
Glucose Metabolic Process
Nadh Regeneration
Dna Replication Dependent Chromatin Organization
Atp Metabolic Process
Dna Packaging
Protein Dna Complex Subunit Organization
Generation Of Precursor Metabolites And Energy
Genesets Size
FDR
H
ATP production rate (pmol/min)
mitoATP
glycoATP
Ly6a WT
Ly6a KO
I
Ly6a WT
Ly6a KO
Genotype
CD137L
Qa-1b
TRAIL-R
CD154
CD48
CD112
H-2Kb
H-2Db
Qa-2
CD155
Rae1
p185 15 WT 1
p185 15 WT 2
p185 13 WT 1
p185 13 WT 2
p185 15 KO 1
p185 15 KO 2
p185 13 KO 1
p185 13 KO 2
J
MFI CD244
Ly6a WT
Ly6a KO
K
% IFN-γ+ cells
Ly6a WT
Ly6a KO
medium
IL-12/15/18
L
MFI granzyme B (gated on granzyme B+ NK cells)
Ly6a WT
Ly6a KO
medium
M
% conjugates
Ly6a WT
Ly6a KO
N
% specific lysis
E:T ratio
Ly6a WT
Ly6a KO

Figure 6

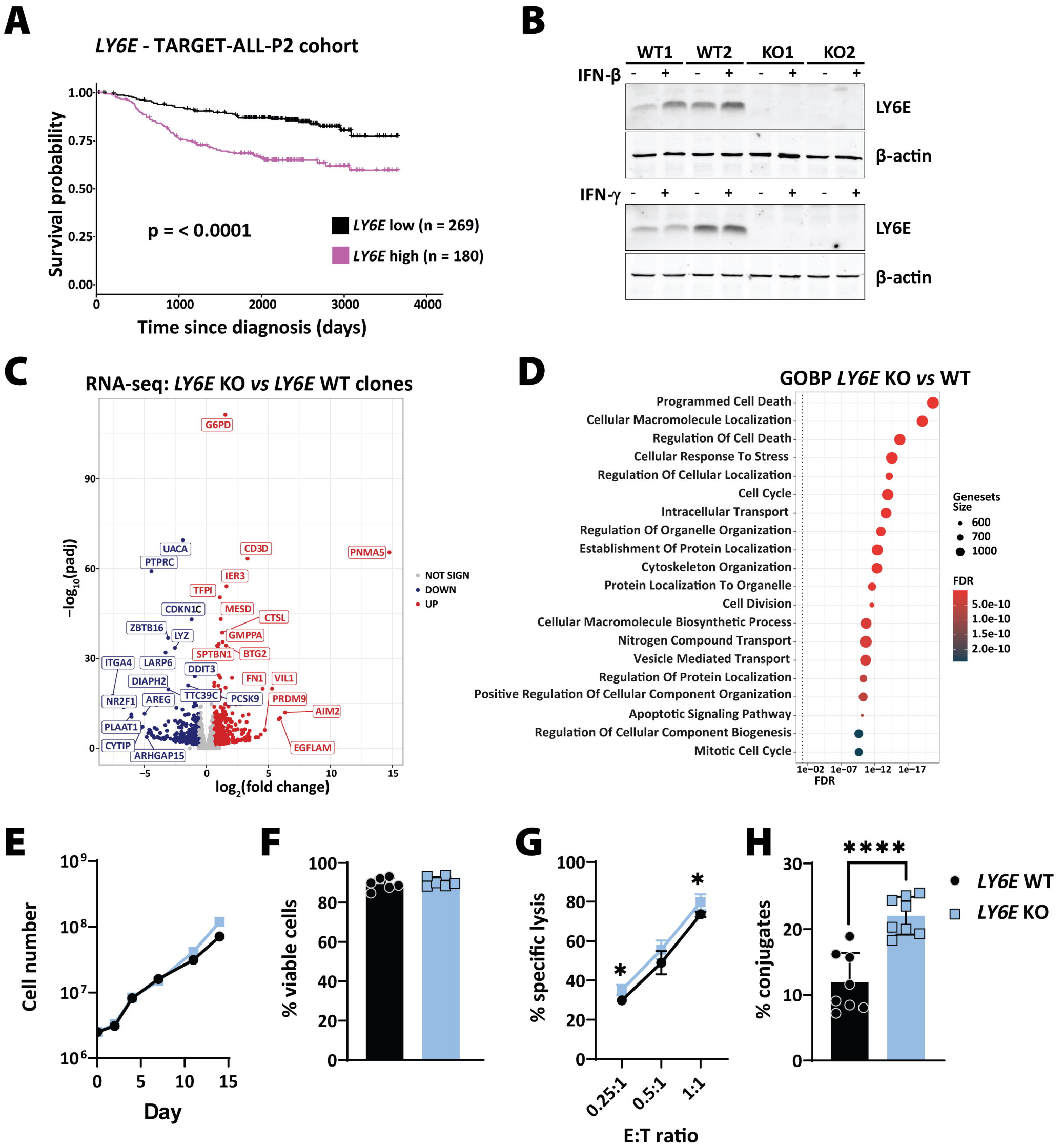
A
LY6E - TARGET-ALL-P2 cohort
Survival probability
1.00
0.75
0.50
0.25
0.00
p = < 0.0001
LY6E low (n = 269)
LY6E high (n = 180)
0
1000
2000
3000
4000
Time since diagnosis (days)
B
WT1
WT2
KO1
KO2
IFN-β
IFN-γ
LY6E
β-actin
C
RNA-seq: LY6E KO vs LY6E WT clones
−log10(padj)
log2(fold change)
NOT SIGN
DOWN
UP
G6PD
UACA
PTPRC
CD3D
PNMA5
IER3
TFPI
CDKN1C
MESD
CTSL
ZBTB16
LYZ
GMPPA
SPTBN1
BTG2
ITGA4
LARP6
DDIT3
DIAPH2
FN1
VIL1
NR2F1
AREG
TTC39C
PCSK9
PRDM9
AIM2
PLAAT1
CYTIP
ARHGAP15
EGFLAM
D
GOBP LY6E KO vs WT
Programmed Cell Death
Cellular Macromolecule Localization
Regulation Of Cell Death
Cellular Response To Stress
Regulation Of Cellular Localization
Cell Cycle
Intracellular Transport
Regulation Of Organelle Organization
Establishment Of Protein Localization
Cytoskeleton Organization
Protein Localization To Organelle
Cell Division
Cellular Macromolecule Biosynthetic Process
Nitrogen Compound Transport
Vesicle Mediated Transport
Regulation Of Protein Localization
Positive Regulation Of Cellular Component Organization
Apoptotic Signaling Pathway
Regulation Of Cellular Component Biogenesis
Mitotic Cell Cycle
1e−02
1e−07
1e−12
1e−17
FDR
Genesets Size
600
700
1000
FDR
5.0e-10
1.0e-10
1.5e-10
2.0e-10
E
Cell number
Day
F
% viable cells
G
% specific lysis
0.25:1
0.5:1
1:1
E:T ratio
H
% conjugates
****
LY6E WT
LY6E KO